WANL-PR(LL)-022
September 30, 1968

DJPJ

Westinghouse Astronuclear Laboratory

SYNTHESIS OF CALCULATIONAL METHODS FOR THE DESIGN AND ANALYSIS OF RADIATION SHIELDS FOR NUCLEAR ROCKET SYSTEMS

Contract No. NAS-8-20414
Contract No. DCN-16-28-0029 (IF)

Volume 2

ANALYSIS OF RADIATION MEASUREMENTS IN A NUCLEAR ROCKET PROPELLANT TANK MOCKUP USING SIMULATED LIQUID HYDROGEN

WANL-PR(LL)-022
September 30, 1968

Westinghouse Astronuclear Laboratory

SYNTHESIS OF CALCULATIONAL METHODS FOR THE DESIGN AND ANALYSIS OF RADIATION SHIELDS FOR NUCLEAR ROCKET SYSTEMS

Contract No. NAS-8-20414
Contract No. DCN-16-28-0029 (IF)

Volume 2

ANALYSIS OF RADIATION MEASUREMENTS IN A NUCLEAR ROCKET PROPELLANT TANK MOCKUP USING SIMULATED LIQUID HYDROGEN

Prepared By:
L. D. Stephenson
R. G. Soltesz
R. K. Disney
S. L. Zeigler

INFORMATION CATEGORY
Unclassified
E. M. Hughley 9/25/68
AUTHORIZED CLASSIFIER DATE

PRECEDING PAGE BLANK NOT FILMED

Astronuclear Laboratory

ACKNOWLEDGMENT

We appreciate the guidance provided by Mr. H. E. Stern, Deputy Manager, Nuclear and Plasma Physics Division, George C. Marshall Space Flight Center, the Technical Monitor of the contract. We also appreciate the efforts of Mr. L. Katz of MSFC in providing the modified propellant tank and associated stress analysis and for performing the safety load test on the tank.

We acknowledge the permission of the Space Nuclear Propulsion Office to perform these measurements in conjunction with NERVA experiments and to utilize certain detector and electronic equipment. We appreciate the review and approval of this work by M. Fleishman, SNPO/Cleveland.

ABSTRACT

This report is Volume 2 of two volumes of the final report on 'Synthesis of Calculational Methods for the Design and Analysis of Radiation Shields for Nuclear Rocket Systems." This work was performed for the George C. Marshall Space Flight Center (MSFC) under Contract NAS-8-20414, Modification 3.

This contract included the measurement and analysis of the radiation environment on and in a modified 72-inch diameter Saturn 1-B LOX tank suspended above a nuclear rocket critical assembly. Measurements were performed at the Westinghouse Astronuclear Experimental Facility (WANEF) with the tank filled with two different densities of polyethylene (0.59 and 0.14 gm/cc) to simulate, respectively, neutron and photon transport properties in liquid hydrogen. A critical mockup of an NRX (NERVA Reactor Experiment) nuclear reactor provided a source of neutron and gamma radiation with the desired spectral characteristics. Two different shield mockups were interposed between the reactor and the propellant tank.

Measurements of neutron fluxes, fast neutron dose rates, and gamma dose rates were made in the propellant tank to provide data on neutron and photon transport properties. Thermal neutron fluxes and neutron spectra on the surface of the tank in a ground test environment were obtained for use in the evaluation of after-shutdown problems associated with activation of the propellant tank structure and for evaluation of radiation analysis methods. Some effects of test cell background were determined experimentally.

Comparisons of calculated and measured neutron and gamma radiation levels are included in this report. The two-dimensional discrete ordinates transport code, DOT, was employed to generate neutron fluxes throughout the reactor assembly; and the data processing code, NAGS, generated source data from those neutron fluxes for use in the point kernel and Monte Carlo analyses. Calculations in the propellant tank were performed utilizing the KAP-V point kernel code and the FASTER Monte Carlo code, both of which were previously provided to MSFC under this contract.

Volume 1 describes the experimental portion of the work, while Volume 2 presents an analysis of these measurements. A classified appendix to Volume 2 presents detailed

geometrical and material descriptions of the reactor and shield mockups and listings of the computer code data employed in this analysis.

TABLE OF CONTENTS

TABLE OF CONTENTS (CONTINUED)

LIST OF ILLUSTRATIONS

LIST OF ILLUSTRATIONS(CONTINUED)

LIST OF TABLES

LIST OF TABLES (CONTINUED)

SECTION 1. INTRODUCTION

This is Volume 2 of a two-volume report on the experimental program carried out in conjunction with the NERVA parametric shield experiments in which a modified Saturn 1B LOX tank filled with simulated hydrogen was placed above the reactor and shield mockup. Presented in this volume are: 1) Conclusions and recommendations; 2) Description of analytical procedures and the results of analysis; and 3) Comparisons of the analytical results with the experimental data described in Volume 1[1]. The analysis was performed using the computer codes provided to Marshall Space Flight Center under Contract NAS-8-20414. The previous work performed under this contract was reported in the nine-volume document, WANL-PR(LL)-010, "Synthesis of Calculational Methods for the Design and Analysis of Radiation Shields for Nuclear Rocket Systems."

This experiment provided measurements of radiation quantities in a propellant tank filled with two different densities of polyethylene to simulate neutron and photon transport characteristics of liquid hydrogen. This experiment was conducted at the WANEF critical facility laboratory above an NRX reactor which provided a radiation source which is almost identical to a flight-type system.

The capability of the calculational methods previously provided to MSFC under Contract NAS-8-20414 to analyze the tank experimental data is demonstrated in this report. In the original contract, a series of comparisons of high-power NRX test data was used as a standard of comparison to indicate the validity of the calculational methods provided to MSFC.

It was evident that little or no experimental data were available for comparison at the dome end of a shielded reactor or in a propellant tank. The PAX (Permanent Assembly Experiment) critical assembly at WANEF employing simulated shield configurations provided basic experimental data which provided an excellent chance to evaluate the calculational methods. A logical extension of this experimental configuration was the inclusion of a simulated

---

[1] Synthesis and Evaluation of Calculational Methods for Design and Analysis of Radiation Shields for Rocket Systems, Volume 1, Radiation Measurements in a Nuclear Rocket Propellant Tank Mockup Using Simulated Liquid Hydrogen, WANL-PR(LL)-022, Vol. 1, September 1968.

propellant tank above the shielded configurations.

The evaluation presented here is limited to those computer codes in the MSFC code package which are applicable to predicting radiation levels in a propellant tank. In addition to providing a basis for evaluation of the current calculational methods supplied to the Marshall Space Flight Center, the work reported herein provides some insight into the application of these computer techniques to the analysis of an actual nuclear rocket reactor experiment. Improvements in the calculational methods which were made since the original contract are also described here.

Section 2 of this volume presents conclusions derived from comparisons of the analytical data with the experimental data and gives recommendations for future analytical method development.

Section 3 describes the application of the two-dimensional discrete ordinate transport code, DOT[2]; the NAGS[3] data processing code; the KAP-V[4] point kernel code; and the FASTER[5] Monte Carlo code to the analysis of the experiments.

Section 4 gives a detailed description of the results obtained employing the above computer codes.

Sections 5 and 6 compare the analytical results with the fast neutron and gamma ray experimental data, respectively.

Section 7 describes the induced activity in the tank wall based upon a prediction from the ACT II (Revised)[6] code and an indication of the radiation levels one might expect around a propellant tank following a full-power operation test.

---

[2] F. R. Mynatt, "A User's Manual for DOT-A Two Dimensional Discrete Ordinates Transport Code with Anisotropic Scattering," K-1694 (In preparation).

[3] Synthesis of Calculational Methods for the Design and Analysis of Radiation Shields for Nuclear Rocket Systems, WANL-PR(LL)-010 Volume 7, June 1967.

[4] IBID, Volume 4

[5] IBID, Volume 9

[6] L. O. Ricks, et al., "Materials Activation Program ACT-II, Revised" WANL-TME-598, November 1963.

Included in this volume, as a classified Appendix, are listings of the KAP-V input data, the FASTER input data, and the POINT, DOT, and NAGS input data. These listings are included so that the problems can be duplicated at the MSFC location.

The classified Appendix to this volume also contains the geometric and material models used in the two-dimensional mockup for the DOT, NAGS, and POINT[7] codes and the KAP-V and FASTER codes.

---

[7] Synthesis of Calculational Methods for the Design and Analysis of Radiation Shields for Nuclear Rocket Systems, WANL-PR(LL)-010, Volume 2, June 1967.

SECTION 2. CONCLUSIONS AND RECOMMENDATIONS

2.1 CONCLUSIONS

A series of comparisons of calculated and experimentally measured neutron and gamma ray radiation levels have been made in a simulated propellant tank. These comparisons were based on the use of the KAP-V point kernel and FASTER Monte Carlo codes with DOT-NAGS neutron and gamma ray sources to calculate these levels. These comparisons include threshold neutron fluxes of E > 2.9 Mev and E > 1.5 Mev; neutron dose rate, and gamma ray dose rate. Agreement is generally good and the following summarizes the comparisons:

1) The FASTER code underpredicts the threshold neutron flux measurements with E > 2.9 Mev and E > 1.5 Mev, FASTER values being a factor of 1.3 to 2.0 lower than measurements at all locations within the tank. This underprediction was noted in the previous scope of work when comparisons with NRX measurements were made. This is attributed to the use of transport corrected cross sections for all elements except hydrogen. The closer agreement of FASTER and experimental values for E > 2.9 Mev at 50 cm into the tank where a considerable amount of hydrogen has been traversed validates this conclusion since hydrogen scattering is treated by a more exact model in FASTER.

2) The KAP-V code using carbon moments data for neutron spectra tends to overpredict the threshold fluxes (E > 2.9 Mev and E > 1.5 Mev) of all locations within the tank. This trend occurs since the KAP-V moments data calculation uses an equivalent carbon penetration for all materials (including hydrogen) in computing spectra. The use of a more sophisticated moments data kernel in KAP-V which employs either a hydrogen or carbon kernel depending upon penetration would improve these results.

3) The KAP-V results on the tank hemisphere and in the traversing tubes are in general agreement as to shape except in the areas close to the tank surface. This disagreement is due in part to the use of infinite media approximation in KAP-V.

4) The FASTER results at the off centerline points and on the centerline of the tank for threshold fluxes tend to predict the correct shape but the values are low as described in 1 above.

5) The KAP-V Albert-Welton and FASTER results for fast neutron dose rate are in excellent agreement on the centerline and at the radial traverses in the tank. This FASTER value agreement is due in part to the fact that the threshold fluxes are underpredicted by FASTER but neutron flux of $E < 1.5$ Mev is overpredicted. At 30 - 50 centimeters into the tank the FASTER values for threshold fluxes are in closer agreement with the experiment and this portion of the spectrum is predominant in dose at this depth penetration into hydrogen.

KAP-V Albert Welton data is in good agreement since the hydrogen penetration is properly handled by the Albert Welton method.

6) The KAP-V carbon moments data values of fast neutron dose rate on the axial centerline of the tank overpredicts since the carbon data does not adequately represent hydrogen scattering of neutrons. This trend was obtained in the previous scope of work and could be improved by use of a better moments method kernel in KAP-V.

7) The KAP-V and FASTER gamma ray dose rate results are in general agreement with the experimental values. Configuration 4B results for CaF_2 TLD experimental values and FASTER and KAP-V results are in general agreement as to shape. FASTER and KAP-V tend to underpredict by approximately 10 to 30 percent, which is, in part, due to not including hydrogen captures in the polyethylene in the calculations. Similar comparisons of the CO_2 active dosimetry results and FASTER and KAP-V indicate similar trends with the experimental values having larger uncertainties. On the axial centerline, the KAP-V results and CO_2 dosimeter values are in excellent agreement as to shape.

8) The KAP-V and FASTER gamma ray results for Configuration 7D are in agreement as to magnitude with the experimental values at the two traversing tube locations. The KAP-V results tend to be higher than FASTER, and this is due, in part, to the large number of FASTER source regions and the poor convergence of these results in the FASTER problems.

2.2 RECOMMENDATIONS

Application of the various computer codes, as reported in Reference 1, to a detailed experiment, results in an accurate definition of additions or improvements which may be made to these techniques. These changes are reflected, not only in the analysis reported here, but also in the continuing application of NERVA-developed computer techniques to the actual design calculations for the NERVA nuclear rocket engine and the total nuclear system, including propellant tanks and payloads. Only during the actual application of these computer techniques do the shortcomings of previously-developed techniques appear. Based upon the application of the POINT, DOT, NAGS, KAP-V, and FASTER programs to the MSFC tank experiment presented in this report, a number of recommended additions and improvements to the MSFC code and data package were noted. These items are listed below:

1) Extend capabilities in the area of discrete ordinate transport techniques by substituting the WANL version of the Oak Ridge National Laboratory code, DOT, in place of the ODD-K[8] code in the MSFC code package. The DOT program, in its present status at WANL, provides for the automated analyses of a complete nuclear stage (reactor, engine, propellant tank, and payload configuration) through the use of the DOT code and the WANL developed MAP II code[9]. The tasks involved in adapting the WANL version of the DOT program system to the MSFC UNIVAC 1108 computer would include the adaptation of the present versions of the WANL NAGS code, DAFT code,[10] and POINT processing codes to the WANL DOT input-output formats and an updated set of users' manuals for these codes.

---

[8] Synthesis of Calculational Methods for the Design and Analysis of Radiation Shields for Nuclear Rocket Systems, WANL-PR(LL)-010, Volume 6, June 1967.

[9] Unpublished

[10] Synthesis of Calculational Methods for the Design and Analysis of Radiation Shields for Nuclear Rocket Systems WANL-PR(LL)-010, Volume 8, June 1967.

2) Incorporate the WANL developed MAP II code into the MSFC code package. The MAP II code, which has been formulated, coded, and applied at WANL, is a technique to reconstruct the angular and energy dependence of the neutron and photon flux as a function of position external to the nuclear subsystem using the reactor surface angular fluxes from the two-dimensional transport code, DOT, as input data. These reconstructed angular fluxes are used automatically as fixed boundary source input to additional DOT two-dimensional transport problems, thus extending the geometrical capability of the DOT program with a minimum amount of computer expenditure. In addition, use of the MAP II code alleviates problems associated with transporting radiation through voids external to the nuclear subsystem. The MAP II code would be made operational on the MSFC UNIVAC 1108 system, and a manual describing the code would be supplied.

3) Analyze the current MSFC tank experiment with the DOT-MAP II technique using the latest developed cross sections. This suggested analysis would not be a repeat of the analysis presented in this report, but would be an extension of this analysis which would provide the consistent application of radiation transport techniques from the nuclear reactor (PAX-E5)through the propellant tank filled with polyethylene. The results obtained to date and presented in this volume indicate the good agreement achieved with the techniques as they have been applied. However, in the area of definition of the radiation environment about a ground test reactor, the capability of calculating the neutron activation of the test cell does not exist in the KAP-V or FASTER codes. The DOT-MAP II technique provides a means to obtain fast and thermal neutron spectra data as a function of position external to the reactor for use in activation. It is recognized, however, that this technique does not provide for a complete analysis of the scattered radiation in the test cell environment.

4) Update the MSFC microscopic neutron library to include additional elements that will be present in nuclear rocket engines and propellant tanks, and include the current improved NERVA cross-section libraries.

During the analysis of NERVA-type reactors, a considerable effort has been expended in the development of cross-section libraries adequate for the nuclear, radiation, and shielding efforts on these reactor designs. This cross-section data is in a continual state of evaluation in the NERVA program, and it is recommended that the current neutron cross-section data be updated according to the latest data for the original 14 elements provided to MSFC, and an additional six elements. A complete cross-section library would be provided for manganese, gadolinium and tantalum, as well as the cross sections for three additional elements to be defined by the contractor. The complete updating of the cross-section library, and the inclusion of additional elements, will provide an extended capability for the analysis of nuclear rocket engines using the present MSFC techniques. Included in the generation of these cross sections is the provision for supplying higher order scattering approximation for gamma ray cross-section data up to a P_3 scatter transfer approximation and the inclusion of up to a P_1 scatter transfer approximation for the neutron data.

5) Modify the NAGS code to include a punched card routine which provides for KAP-V and FASTER source data in punched card form for direct use in these two codes. This addition eliminates the large amount of data preparation required to use NAGS sources. A simple modification the KAP-V program is needed in order to use the large data arrays generated by NAGS. The KAP-V program has the capability of using source distribution data with a large number of values to interpolate to a source distribution adequate for this analysis. The entry of these data for source interpolation is limited to 21 in the current MSFC code package. A value of 51 was needed to handle the detailed geometrical description used in the analysis of Configuration 7D of this experiment analysis.

6) Modify the FASTER code to allow the entry of the starting random number and the available data storage locations in the FASTER code. This modification would allow the use of the FASTER code on the UNIVAC 1108 computer in a more efficient manner.

7) Incorporate the one-dimensional discrete ordinate transport code, ANISN[11], as the one-dimensional discrete ordinate transport technique in the MSFC code

[11] W.W. Engle, Jr., "A User's Manual for ANISN - A One-Dimensional Discrete Ordinate Transport Code with Anisotropic Scattering" K-1693, March 1967.

package. (The ANISN program and DOT program are similar in nature.) ANISN would replace the TAPAT code system. Some programming effort is required on the ANISN code to duplicate the TAPAT capability in its entirety. The capability of the one-dimensional discrete ordinate transport technique would be greatly increased because ANISN is coded in FORTRAN IV with complete variable dimensioning for data storage.

8) Provide a set of 25 group neutron cross sections for the FASTER Monte Carlo code which are consistent with those used in the discrete ordinate transport codes. It is recommended that a fine group cross section set be applied in the high energy range; i.e., $E > 0.1$ Mev. This cross-section library would include not only the transport corrected cross sections similar to the ones that are used in the discrete ordinate transport codes, but also the scatter cross sections in up to a P_3 approximation.

9) Extend the capability of the KAP-V code in the areas of: a) a more sophisticated application of neutron moments data, and b) the inclusion of multiple-layer gamma ray buildup approximations.

The modification to the KAP-V program to improve its neutron calculation would be in the area of applying the neutron moments data polynomial coefficients in a fashion such that the penetration through carbon, polyethylene, hydrogen, or other materials of dissimilar neutron transport characteristics could be handled simultaneously in the KAP-V program. This "multiple" moments calculation would increase the capability of the KAP-V code for analyzing nuclear rocket-propellant tank geometries. Modifications to the KAP-V to include multiple-layer gamma ray buildup approximation would allow for analysis of thick shield geometries without relying on the intuition of the user in selecting a single representative set of buildup factor data.

10) Develop a flexible activation code, based on the WANL ACT II code (Revised) to handle reactor test power profiles, gamma and beta activity, and dose rate levels at any time during or following nuclear rocket tests. This code would facilitate test stand and vehicle activation analysis.

SECTION 3. METHODS OF ANALYSIS

3.1 INTRODUCTION

In the previous work scope of this contract, a series of computer codes, which are described in detail in Volumes 1 through 9 of WANL-PR-(LL)-010 were provided as a complete package to analyze the radiation environment around the NERVA nuclear stage. These procedures, or codes, included the radiation transport methods of discrete ordinates transport in one and two-dimensions, a point kernel attenuation code, and a Monte-Carlo code, as well as data processing techniques required to prepare input for the various codes. The analytical procedures were selected primarily on the basis of their flexibility and utility in the analysis of nuclear rocket radiation environments. For this experimental analysis, the POINT code was used for the preparation of cross-section data for input into the two-dimensional DOT, Discrete Ordinates Transport, code (the DOT program was selected with the concurrence of Mr. H. Stern, the contract monitor, to replace ODD-K as the two-dimensional discrete ordinates transport method), the NAGS code was used to perform the necessary data processing tasks employing as input the DOT neutron flux data and the POINT code cross-section data, and the KAP-V and FASTER codes were used to calculate radiation environment using the NAGS source distribution data.

This section describes the techniques used in each phase of the experiment analysis of the PAX-E5 assembly as well as the use of the DOT code as it was applied, the application of the NAGS source distribution data into KAP-V and FASTER, and the other data used in KAP-V and FASTER. Included in the description of the analytical procedures is a brief description of the differences between the currently used POINT, NAGS, KAP-V and FASTER codes and the code package supplied to MSFC. The current versions of these codes were used because the modifications made to the codes facilitated description of the detailed experimental model in the codes. Since it was felt that these techniques should be applied to the best of their capability in order to analyze properly the experiment in as fine a detail as possible under the current work scope, the improved or changed versions of the codes were used in deference to the original versions. The primary changes made to these codes have been in the nature of data processing improvements, such that the linkage between codes

was an improved automated procedure over the original MSFC code package. These changes reflect the types of improvements one must go through as a computer code package is expanded and modified.

3.2 DESCRIPTION AND USE OF THE TWO-DIMENSIONAL DISCRETE ORDINATE TRANSPORT METHOD (POINT, DOT, NAGS)

In the time span since the original contract and during the analysis of the current tank experiment, considerable advances have been made in the discrete ordinate transport techniques available for use in the analysis of NERVA-type reactors. Many of these advances have been incorporated in the two-dimensional transport code, DOT. This code which was obtained from the Oak Ridge National Laboratory in early 1967, has been appropriately modified and placed on an operational status in the current version of the code at WANL. This code has the capability of completely replacing the ODD-K code in the MSFC code package and in the best interest of keeping the MSFC code package current with generally accepted techniques, the analysis of the tank experiment radiation source, that is, the PAX assembly, was carried out using the DOT code and the data processing links, POINT and NAGS as provided under the original MSFC contract work. Hence, the objective of the MSFC tank experiment analysis was to provide a real application of the POINT-DOT-NAGS computer codes to a critical experiment reactor, and using the photon source and neutron source data generated using the DOT-NAGS linkage, calculate the radiation environment in a simulated propellant tank using the FASTER and KAP-V Codes.

The approach to the analysis of the MSFC tank experiment is diagrammed in Figure 3-1. This flow chart illustrates the linkage of the computer codes used to analyze the different reactor-tank simulations. This analysis procedure, which involves the use of the POINT data processing code, the DOT two-dimensional discrete ordinate transport code and the NAGS data processing code, provided detailed source data for the KAP-V point kernel and FASTER Monte Carlo attenuation codes. This procedure was used as an automated technique to the extent that magnetic data tapes and punched data cards prepared by the individual codes passed the appropriate information to succeeding phases of analysis as indicated in the

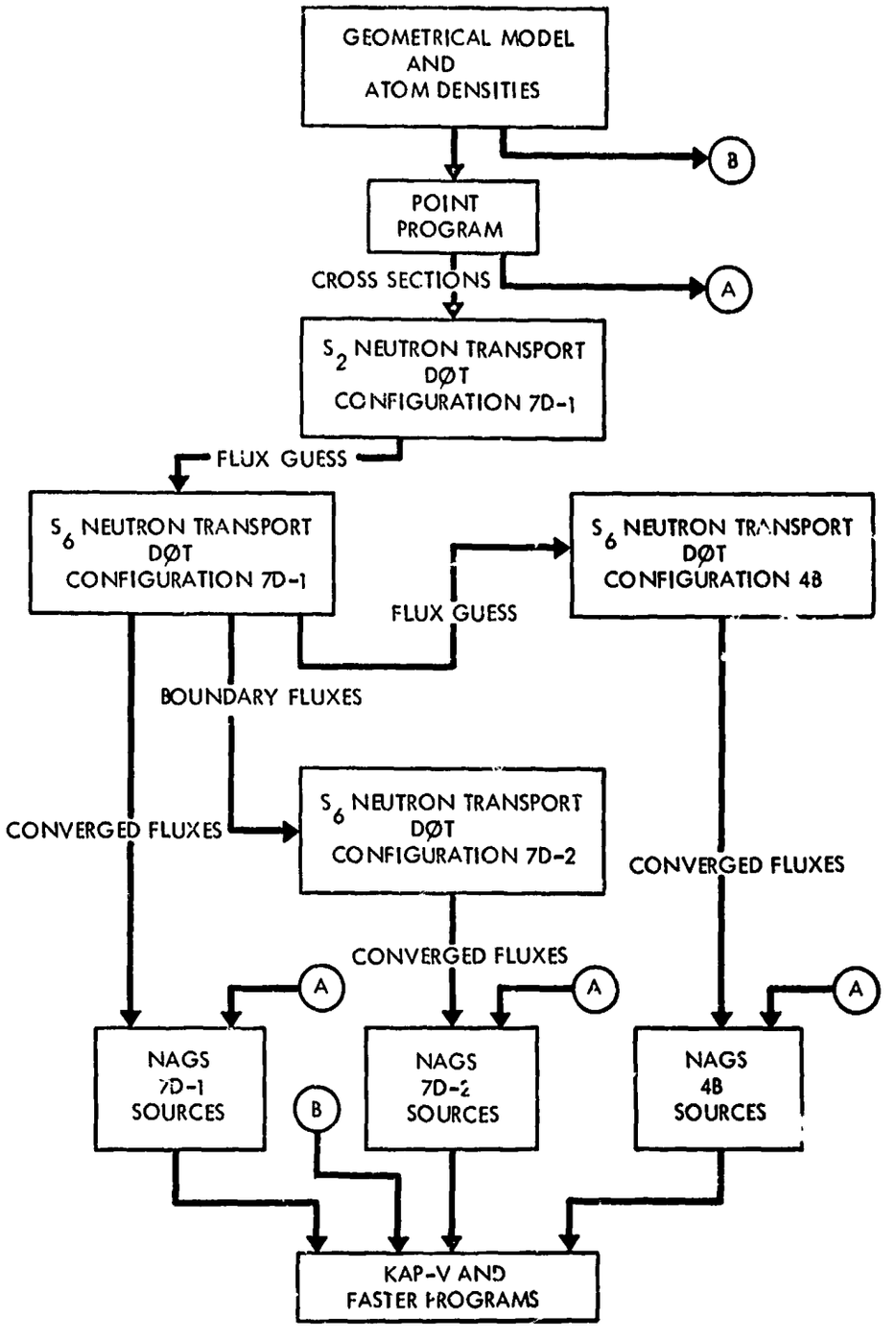

Figure 3-1. Flow Diagram for Two-Dimensional Transport Analyses of MSFC Experiments

flow diagram. This flow diagram is similar to Figure 4-7 of Reference 1 with the exception of the use of DOT and its extended capabilities. The use of each individual code is described in following sections.

POINT Code

The POINT code as described in Volume 2 of Reference 1 was used to provide macroscopic neutron transport cross sections, and microscopic neutron reaction data for use in the DOT and NAGS codes. As shown in Figure 3-1, the geometrical descriptions and element atom densities derived from the geometrical models in the classified Appendix A to Volume 2 were used in the POINT Program. The resulting punched neutron transport cross sections and neutron reaction data libraries were used as input data to the DOT and NAGS codes respectively. Three additional elements were included in the POINT library for this analysis. A complete listing of the revised library is given in Appendix A.

DOT Code

The DOT code was used to calculate multigroup neutron flux distributions in the two experimental configurations. As shown in Appendix A, configuration 7D was split into two DOT problems; 7D-1 which contained the reactor assembly geometry and shield slab mockups up to and including one shield module; and 7D-2 which represented all six shield modules, the plena, and pressure vessel mockups. As shown in Figure 3-1, the first DOT problem, 7D-1, was run as an S_2-P_o eigenvalue calculation containing 2574 mesh cells. The converged fluxes from this calculation were then input by magnetic tape into the next DOT problem, 7D-1, which was an S_6-P_o eigenvalue calculation. As shown in Figure 3-1, the converged fluxes from this problem were used for three purposes: 1) as input fluxes for the NAGS problem, 7D-1, 2) as a flux guess for the DOT problem 4B, and 3) as a boundary source for DOT problem, 7D-2. Problem 4B was an S_6-P_o eigenvalue calculation as well, containing 2457 mesh cells and was quite similar to 7D-1 except that no shield modules were present and the plena and pressure vessel mockup slabs were included next to the core support plate mockup slabs. Converged fluxes from problem 4B were then input into the NAGS problem for configuration 4B via magnetic tape. By using the automated boundary source

option in the DOT program, the boundary angular fluxes from DOT problem 7D-1 at an internal mesh interval were used as the boundary source for problem 7D-2. This source was obtained as an energy function of space, angle, and radial mesh interval at the fifty-first axial mesh interval in the DOT problem 7D-1. This problem was a fixed boundary source type calculation in DOT and requires only one outer iteration where flux convergence is achieved on inner iterations. A total of 4,017 mesh cells and 30 space angles (S_6) were used in problem 7D-2. The eigenvalue for the PAX-E5 critical assembly using the MSFC library cross sections was calculated to be 1.002 for both configurations 4B and 7D using an overall eigenvalue convergence criteria of 0.001 and a maximum pointwise flux convergence criteria of 0.005 in all three DOT problems. The converged flux tape from problem 7D-2 was inverted with respect to axial interval (the geometry for 7D-2 is inverted in the Z direction with respect to 7D-1 because DOT requires a boundary source from the top boundary of the system) using a small utility program, and then input into the NAGS problem for configuration 7D-2.

With such a complex system as existed in configuration 7D, the original discrete transport code, ODD-K, could not adequately represent the system in sufficient detail to yield meaningful results. As available in the WANL version of DOT, an automated boundary source option allows for as many as three or four coupled DOT problems if desired to analyze configurations such as 7D introducing less than a few percent error at the boundaries. The WANL version of the DOT code is directly compatible with the WANL NAGS code by employing tapes as connecting data set links. The WANL version of DOT has the capability of generating a flux tape for NAGS (neutron or photon) as well as the provision for reading the fixed distributed source tape generated by NAGS directly. For equivalent input data sets, DOT calculates the same results as ODD-K within the convergence criteria chosen.[12]

NAGS Program

The NAGS code described in Volume 7 of Reference 1 was used in this analysis to provide neutron and photon source distributions for direct input into the KAP-V point

---

(12) WANL-TME-1680, "Status Report on the Conversion (for a CDC Computer) of the Two Dimensional Transport Program DOT", September 1967.

kernel code and the FASTER Monte Carlo code. As shown in Figure 3-1, all three DOT problem converged flux tapes for configurations 7D-1, 7D-2, and 4B were input to NAGS in units of neutrons/cm^2-sec-source neutron. In the NAGS code, the fluxes were normalized to units of (neutrons/cm^2-sec-watt) using the conversion factors as shown in the listings of the NAGS problems given in Appendix A. Photon sources, obtained from NAGS as printed and punched data cards, for KAP-V and FASTER were obtained in units of (Mev/cm^3-sec-watt). The axial dimensions used in the NAGS problems were shifted by a constant in NAGS so that the punched source distribution coordinates would correspond exactly with the KAP-V and FASTER geometrical models. This automated punch routine in NAGS allowed for the consistent use of source data in KAP-V and FASTER.

3.3 DESCRIPTION AND USE OF THE MONTE CARLO METHOD (FASTER)

The FASTER code which is described in Volume 8 of WANL-PR(LL)-014[13] was used for the prediction of neutron and gamma radiation levels in the simulated propellant tank. The code used was essentially the MSFC code package with two minor modifications made at WANL to facilitate running problems with different initial random numbers and to allow for the large problems encountered in analysis of Configuration 7D. With these exceptions the use of FASTER for the analysis was as described in the user's manual for the FASTER code.

The present WANL version of FASTER is coded such that at the completion of any single run, the number of random numbers used in the calculation of all detectors in the problem is printed out as final data. This total number of random numbers can then be used as an input quantity to subsequent FASTER runs so that randomness of the numbers used in the FASTER problems can be preserved in sequential FASTER problems. In addition to the capability of inputting the sequence number of the starting random number, the WANL version of FASTER has been altered such that the number of data locations to be used for all data is an input quantity on the first data card. This is an extremely useful option for computer facilities where

---

[13] Computer Code Symposium, Synthesis of Calculational Methods for the Design and Analysis of Radiation Shields for Nuclear Rocket Systems, WANL-PR(LL)-014, Volumes 1-9, December 1967.

extended core capabilities are available. At WANL, there exist two sizes of CDC 6600 computers and the input of this computer does not require a recompilation of the FASTER code.

With the exception of source terms, geometrical descriptions, material descriptive data and response functions, the FASTER input data used for the analysis of the tank experiments are the same as presented in WANL-PR(LL)-010, Volume 9. These data include the neutron and gamma ray cross sections, biasing parameters, and code options to be used in the execution of the FASTER problems. In the review of these data in the current MSFC FASTER problem deck, two errors were noted and have been corrected for the present analysis. These errors were: 1) the nonelastic cross sections for group 7 through 9 for uranium 235 were not in the correct sequence, and 2) the P_o within group scatter cross sections for titanium were missing. These data have been corrected and the listing of the data for the FASTER problems reflect these changes. This listing appears in the Appendix to this volume.

Geometry Description

The analysis using the FASTER code consisted of three individual problems as follows:

Problem 1: The neutron problem using volume distributed neutron sources from the DOT-NAGS codes to calculate the neutron radiation environment in the propellant tank for configuration 4B, as shown in Figure A-9 of Appendix A.

Problem 2: The gamma ray problem using the volume distributed photon sources from the DOT-NAGS codes to calculate gamma environment in the propellant tank for configuration 7D as shown in Figure A-8 of Appendix A.

Problem 3: The gamma ray problem using the volume distributed photon sources from DOT-NAGS codes to calculate gamma environment in the propellant tank for Configuration 4B as shown in Figure A-9 of Appendix A.

The geometry model for these three FASTER problems are shown in Figures A-8 and A-9 in the classified appendix to this volume. The regions described in the reactor are shown in the figures and the composition of each zone is shown in Table A-17. The geometry is identical with the one used for the KAP-V point kernel analysis with the exception that external zones 44, 45, 46, and 47 in Figure A-8, and external zones 42, 43, 44, and 45 in Figure A-9 are needed in the KAF problems. The FASTER code does not require the definition of any external zone for this analysis.

To simplify the setup of a problem as complex as Configuration 7D, or Configuration 4B, one must recognize the various limits which are imposed on the FASTER source input data description and set the geometry model based on these data. In the running of the neutron transport problem in the DOT two-dimensional transport code, the definition of explicit zones for: 1) the highly absorbing boron regions, 2) the highly neutron attenuating polyethylene regions, and 3) the metallic slab regions in the flight shield mockup create a large number of zones to be used in the source description. In FASTER a source zone in a geometrical region must completely cover that region or the FASTER code will extrapolate source data to the region bounds. If a source zone is a small region within a physical region then the user of FASTER (to properly use DOT-NAGS source data) must define a new physical region which is no larger than the source region. Since the DOT program was run with 63 source regions, the FASTER input data and geometry description included all zones in the DOT problems. The FASTER geometry which is shown in Figures A-8 and A-9 of the Appendix reflects only the compositional model of the geometry. Internal to regions 30, 31, and 32, a series of subregions were provided with identical composition, but with boundaries corresponding to DOT problem source descriptions. This FASTER model allowed direct use of source data from the WANL NAGS code and resulted in a total of 81 surfaces and 83 regions to describe the geometry for the DOT-NAGS sources.

Material Description

The technique used in the FASTER model description was to homogenize the flight shield mockup into a single composition comprised of titanium, aluminum, inconel, polyethylene, and boral. This composition was then assumed to be in each subregion of the

physical shield region. These subregions had dimensions identical to the DOT-NAGS source regions.

The total number of elements used to mockup the MSFC tank experiment in FASTER was 14 since various similar minor constituents were combined as described in Appendix A to reduce the total number of elements. The total number of compositions in the FASTER problems was 33 which included all compositions which were encountered in either the 4B or 7D geometry, and in addition, a 0.07 gram/cm^3 dense hydrogen composition was defined in one region of the gamma ray FASTER problem in order to obtain heating rate response in liquid hydrogen.

Source Description

The source data input to the FASTER problems consisted of the upper and lower energies (in Mev) for each of 15 neutron energy groups and 23 gamma groups as shown in Tables 3-1 and 3-2. The neutron energy breakpoints are consistent with GAM-II* cross section library data included in the MSFC FASTER code package.

Since the FASTER program employs interpolation techniques to handle source energy data in group structures other than shown in Tables 3-1 and 3-2, the entry of DOT-NAGS data in the 13 group scheme shown in Table 3-3 is possible. The technique used in specifying neutron source data in FASTER was to use the GAM II fission neutron spectrum as shown in Table 3-4. Hence, the technique of using the neutron source for each of nine core regions as neutron/cm^3-sec-watt for each region was possible. Neutron source distribution data from NAGS in the form of radial and axial distributions for each region were also used. This source description is totally consistent with the KAP-V analysis.

The technique for the entry of gamma ray data for each source region in Configurations 7D and 4B was handled in a similar manner except that the total gamma source in each region in units of Mev/cm^3-sec and the spectrum for each source region was specified. Source distribution was the gamma ray data from NAGS. Source data were uniform in azimuth and

* This cross section data was obtained from Mr. G. Lahti, Lewis Research Laboratory, Cleveland.

TABLE 3-1

ENERGY GROUPS FOR THE FASTER NEUTRON PROBLEM

Group	Upper Energy (Mev)	Lower Energy (Mev)	Average Energy (Mev)
1	14.918	10.0	11.26
2	10.0	7.4082	8.45
3	7.4082	6.0653	6.71
4	6.0653	3.6788	4.56
5	3.6788	2.7253	3.14
6	2.7253	2.2313	2.46
7	2.2313	1.108	1.57
8	1.108	0.82085	0.956
9	0.82085	0.6081	0.709
10	0.6081	0.40762	0.50
11	0.40762	0.30197	0.352
12	0.30197	0.18316	0.237
13	0.18316	0.11109	0.144
14	0.11109	9.1188×10^{-3}	0.0374
15	9.1188×10^{-3}	9.14×10^{-7}	1.5×10^{-3}

TABLE 3-2

GROUP STRUCTURE FOR FASTER GAMMA RAY CROSS SECTION DATA

Group	Upper Limit (Mev)	Lower Limit (Mev)
1	10.0	9.0
2	9.0	8.0
3	8.0	7.0
4	7.0	6.0
5	6.0	5.0
6	5.0	4.0
7	4.0	3.0
8	3.0	2.5
9	2.5	2.0
10	2.0	1.75
11	1.75	1.5
12	1.5	1.25
13	1.25	1.0
14	1.0	0.8
15	0.8	0.6
16	0.6	0.4
17	0.4	0.3
18	0.3	0.2
19	0.2	0.1
20	0.1	0.08
21	0.08	0.06
22	0.06	0.04
23	0.04	0.03

TABLE 3-3

FASTER GAMMA RAY SOURCE ENERGY GROUP STRUCTURE

Group	Upper Energy (Mev)	Lower Energy (Mev)
1	10.0	7.5
2	7.5	7.0
3	7.0	6.0
4	6.0	5.0
5	5.0	4.0
6	4.0	3.0
7	3.0	2.6
8	2.6	2.2
9	2.2	1.8
10	1.8	1.35
11	1.35	0.9
12	0.9	0.4
13	0.4	0.0

TABLE 3-4

FASTER FISSION NEUTRON SPECTRUM

g, Neutron Group No.	χ_g, (Neutrons/Fission Neutron)
1	1.0407 (-3)
2	7.2417 (-3)
3	1.4934 (-2)
4	1.0825 (-2)
5	1.1814 (-1)
6	9.2319 (-2)
7	3.1165 (-1)
8	1.0024 (-1)
9	7.6058 (-2)
10	6.9540 (-2)
11	3.4031 (-2)
12	3.4042 (-2)
13	1.7143 (-2)
14	1.5365 (-2)

directional emission for all FASTER calculations. The source data for FASTER is presented in the data listing in Appendix A.

Response and Detector Coordinate Description

The final set of FASTER data used is the response data and detector coordinates. Response data for neutrons and gammas are presented in Tables 3-5 and 3-6 for the neutron and gamma problems. These responses were internally calculated by FASTER for heating response and the dose rate response were entered as shown in the tables. Detector point locations are described in detail in Section 4.

3.4 DESCRIPTION AND USE OF THE POINT KERNEL METHOD (KAP-V)

The KAP-V code, which is described in detail in Volume 4 of WANL-PR(LL)-010, was used in a similar fashion to the FASTER code to predict fast neutron and gamma radiation levels in the propellant tank. Since the point kernel method uses a direct analytical calculation of the radiation attenuation in a geometry model, the code, the used to provide much greater detail (i.e., more detectors) than the FASTER Code. Application of KAP-V to the analysis of the two experimental configurations, 7D and 4B, and the MSFC tank experiments were identical and similar data options were used. The exceptions to the MSFC code package were the direct use of source data from the NAGS alteration of the geometry to the PAX reactor, and the inclusion of additional response functions for comparison to the measured experiment values.

Geometry Description

The analysis using the KAP-V program consisted of two individual problems to mockup the configuration 7D and configuration 4B, respectively. Since the capability of the KAP-V code includes both neutron and gamma ray solutions for essentially the same computer time expenditure, the neutron and gamma ray problem for both configurations were run in the problems. The two problems and their geometries are shown in Appendix A. The regions described in the reactor are as shown in the figures and the composition of the tables are consistent with the FASTER analysis. The geometry model for use in the KAP-V is

TABLE 3-5

FASTER NEUTRON RESPONSE DATA

Group	Energy (Mev) Upper	Energy (Mev) Lower	Dose Rate Rem/Hr	Dose Rate Rads (Tissue) / Hr	Dose Rate Rads (Ethylene)/Hr	Energy Deposition Rate* Mev/sec-cm^3 of CH_2 (ρ = 0.59 gm/cm^3)
1	14.92	7.41	1.15 (-4)	1.80 (-5)	2.70 (-5)	3.38 (-1)
2	7.41	6.06	1.15 (-4)	1.80 (-5)	2.70 (-5)	2.41 (-1)
3	6.06	3.68	1.07 (-4)	1.65 (-5)	2.30 (-5)	2.54 (-1)
4	3.68	2.72	1.10 (-4)	1.60 (-5)	2.15 (-5)	2.05 (-1)
5	2.72	2.23	9.50 (-5)	1.28 (-5)	1.90 (-5)	1.82 (-1)
6	2.23	1.11	9.50 (-5)	1.13 (-5)	1.62 (-5)	1.81 (-1)
7	1.11	0.82	9.00 (-5)	8.60 (-6)	1.13 (-5)	1.17 (-1)
8	0.82	0.608	7.40 (-5)	7.20 (-6)	1.00 (-5)	1.07 (-1)
9	0.608	0.408	6.50 (-5)	6.20 (-6)	9.00 (-6)	9.37 (-2)
10	0.408	0.302	5.40 (-5)	5.20 (-6)	7.40 (-6)	7.45 (-2)
11	0.302	0.183	4.00 (-5)	4.00 (-6)	5.80 (-6)	6.59 (-2)
12	0.183	0.111	3.30 (-5)	3.40 (-6)	5.00 (-6)	4.65 (-2)
13	0.111	4.14 (-7)	2.10 (-5)	2.50 (-6)	3.60 (-6)	3.87 (-2)
	4.14 (-7)	----	0.0	0.0	0.0	2.15 (-7)

*Energy deposition factors apply to group upper end point energy. To obtain energy deposition rate in Btu/sec-in^3, multiply by 2.5×10^{-15}

TABLE 3-6

FASTER GAMMA RAY RESPONSE DATA

Group Upper End Point Energy (Mev)	Dose Rate Rads (Carbon)/Hr	Dose Rate Rads (Tissue)/Hr	MeV/Sec-cm3 of LH_2^*	Mev/Sec-cm^3 of CH_2^* (ρ = 0.14 gm/cm^3)	Mev/Sec-cm^3 of CH_2^* (ρ = 0.59 gm/cm^3)
10.0	8.37 (-6)	9.76 (-6)	1.57 (-2)	2.19 (-2)	9.23 (-2)
8.0	7.04 (-6)	7.79 (-6)	1.41 (-2)	1.87 (-2)	7.87 (-2)
6.0	5.75 (-6)	6.33 (-6)	1.22 (-2)	1.55 (-2)	6.52 (-2)
4.0	4.39 (-6)	3.79 (-6)	9.91 (-3)	1.20 (-3)	5.04 (-2)
2.5	3.18 (-6)	3.50 (-6)	7.54 (-3)	8.78 (-3)	3.70 (-2)
1.75	2.47 (-6)	2.58 (-6)	6.03 (-3)	6.93 (-3)	2.92 (-2)
1.25	1.91 (-6)	2.08 (-6)	4.66 (-3)	5.02 (-3)	2.11 (-2)
0.8	1.39 (-6)	1.44 (-6)	3.22 (-3)	3.70 (-3)	1.56 (-2)
0.4	6.82 (-7)	7.39 (-7)	1.65 (-3)	1.89 (-4)	7.96 (-3)
0.2	3.07 (-7)	3.38 (-7)	7 41 (-4)	8.49 (-4)	3.58 (-3)
0.08	9.32 (-8)	1.53 (-7)	2.02 (-4)	2.51 (-4)	1.06 (-3)
0.03	1.07 (-7)	3.34 (-7)	3.87 (-5)	2.25 (-4)	9.47 (-4)

*To obtain energy deposition rates in Btu/sec-in^3, multiply by 2.5×10^{-15}

identical to the FASTER model with the exception that the external zones of the geometry are necessarily described for the KAP-V program. Since the KAP-V calculation is initiated in a source region and the ray tracing through the geometry is performed to the detector point, the inclusion of extra subregions to describe the DOT-NAGS source description was not necessary. The technique used in the KAP-V code was identical to the FASTER code except that source regions need not be described in KAP-V but rather the source region calculation is included in the physical region and the calculation proceeds from the source point to the detector point.

Source Description

The preparation of source data for KAP-V is similar to that for the FASTER code described earlier. In the neutron point kernel problem, the definition of the source zones did not pose as much a problem as that of FASTER since the source regions could simply be placed in a physical region without new boundaries. The same source region data and source description as used in the FASTER program was employed in the KAP-V program and a total of 63 source regions were used in the KAP-V 7D configuration analysis and the total of 33 sources were employed in the KAP-V configuration 4B analysis. Since the neutron and gamma ray calculations are carried out simultaneously in the KAP-V program, there were a total of 9 neutron source regions used in the KAP-V problem in addition to the 63 and 33 gamma ray source data regions for configurations 7D and 4B, respectively. The source data used in the KAP-V analysis were prepared automatically by the WANL NAGS code and these punched data were then used directly in the KAP-V problem deck.

The WANL version of KAP-V was changed to provide the capability of using the NAGS generated data directly. As described in Section 3.2, the NAGS code was altered to provide as punched output complete source description data for both the KAP-V and FASTER code. This source data, because of the complexity and size of the reactor model, required an extension of certain input data arrays in the KAP-V code in order to allow direct NAGS input. The source distribution data for the interpolated data, which is known as the data

quantity FSIT, was altered in the program such that 51 values of source distribution data could be entered by the user. This change allowed direct use of NAGS data in KAP-V and provided a very consistent application of the KAP-V and FASTER codes using NAGS generated data.

Since a detailed description of the data in KAP-V and the use of KAP-V sample problem was included in Reference 2 the details of the input will not be covered in this report except to discuss the actual input data prepared for these analysis. A portion of the KAP-V input data is summarized in Tables 3-7 through 3-12.

Gamma Ray Library Data

The gamma ray cross section library data are shown in Table 3-7. The option used in KAP-V allowed the program to calculate total gamma ray mass absorption coefficients for the 14 elements in the gamma ray library as shown in Table 3-7 at the average energy shown in Table 3-7. These data are consistent with the FASTER model and the energy grouping is consistent with the NAGS energy group structure.

Neutron Input Data

The neutron cross section data for both the neutron moments data calculation and the Albert-Welton calculation in KAP-V is shown in Table 3-8. These data are identical to those presented in the MSFC Code package and additional elements were added for this analysis. The energy breakpoints and polynomial coefficient data for use in the neutron ten energy point moments data calculation are shown in Tables 3-9 and 3-10, respectively. These data indicate the energy at which the number flux from the neutron moments data calculation was obtained. Associated with each of these energy points is an energy band width to be used in the integration of this differential neutron spectra to obtain either total number flux or energy response. Since the carbon moments data is an empirical fit over the depth penetration ranges of 0 to 60 grams per square centimeter of equivalent carbon depth penetration and 60 to 120 grams per square centimeter depth penetration, the inclusion of extrapolation parameters far beyond 120 gm per square centimeter as a function of each group are provided in the KAP-V

TABLE 3-7

INPUT DATA FOR GAMMA RAY LIBRARY

Material No.	Element Name	Z Atomic No.
1	H	1
	C	6
3	U-235	92
4	U-238	92
5	Nb	41
6	Ni	28
7	Cr	24
8	Fe	26
9	Ni	22
10	Ti	29
11	Cu	13
12	Al	42
13	Mo	4
14	Be	5

Gamma Ray Group No.	Average Energy (Mev)
1	8.50 (0)*
2	7.25 (0)
3	6.50 (0)
4	5.50 (0)
5	4.50 (0)
6	3.50 (0)
7	2.80 (0)
8	2.50 (0)
9	2.00 (0)
10	1.50 (0)
11	1.00 (0)
12	7.00 (-1)
13	3.00 (-1)

*Numbers in parenthesis refer to powers of 10.

TABLE 3-8

NEUTRON CROSS SECTIONS AND DATA FOR THE ALBERT-WELTON KERNEL FOR KAP-V

Material No.	Name	Σ^*_{A-W}	η	Σ_R^*
1	H	0	8.688	6.0 (-1)
2	C	4.07 (-2)**	0.0	4.07 (-2)
3	U-235	9.1 (-3)	0.0	9.1 (-3)
4	U-238	9.1 (-3)	0.0	9.1 (-3)
5	Nb	1.6 (-2)	0.0	1.6 (-2)
6	Ni	1.9 (-2)	0.0	1.9 (-2)
7	Cr	2.17 (-2)	0.0	2.17 (-2)
8	Fe	2.1 (-2)	0.0	2.10 (-2)
9	Ti	2.2 (-2)	0.0	2.2 (-2)
10	Cu	1.8 (-2)	0.0	1.80 (-2)
11	Al	2.9 (-2)	0.0	2.9 (-2)
12	Mo	1.56 (-2)	0.0	1.56 (-2)
13	Be	7.2 (-2)	0.0	7.2 (-2)
14	B	5.8 (-2)	0.0	5.8 (-2)

Albert-Welton Constants	Value
α_1	1.6 (-4)
α_2	2.9 (-1)
α_3	7.78 (-1)
α_4	5.8 (-1)
α_5	3.5 (-5)
α_6	1.0 (1)
α_7	9.58 (-2)
AWSOUR	(Dependent upon source region in core)

* $cm^2/gram$

** Number in parenthesis refers to powers of ten.

TABLE 3-9

MONOVARIANT NEUTRON MOMENTS DATA ENERGY POINTS

Group No.	E, Energy (Mev)	ΔE (Mev)
1	18.0	4.0
2	14.0	4.0
3	10.0	3.0
4	8.0	2.0
5	6.0	2.0
6	4.0	1.5
7	3.0	1.0
8	2.0	1.0
9	1.0	0.85
10	0.33	0.565

TABLE 3-10

MONOVARIANT NEUTRON MOMENTS DATA* FOR CARBON

Neutron Group No.	A0	A1	A2	A3	A4
			Coefficients for $W < 60$ gm/cm^2		
1	2.243(-05)**	-2.696(-03)	1.061(-01)	-1.695(0)	-4.573(0)
2	1.820(-05)	-2.171(-03)	8.425(-02)	-1.325(0)	-3.443(0)
3	1.179(-05)	-1.416(-03)	5.577(-02)	-9.057(-01)	-2.353(0)
4	9.022(-06)	-1.081(-03)	4.246(-02)	-6.969(-01)	-1.833(0)
5	6.743(-06)	-8.052(-04)	3.131(-02)	-5.105(-01)	-1.333(0)
6	3.968(-06)	-4.599(-04)	1.702(-02)	-2.814(-01)	-8.700(-01)
7	2.099(-06)	-2.419(-04)	8.718(-03)	-1.564(-01)	-6.567(-01)
8	1.846(-06)	-1.990(-04)	5.997(-03)	-8.101(-02)	-4.767(-01)
9	2.640(-08)	-3.806(-06)	-6.236(-04)	2.448(-02)	-3.533(-01)
10	-8.848(-07)	1.108(-04)	-5.279(-03)	9.816(-02)	-3.733(-01)
			Coefficients for $60 < W < 120$ gm/cm^2		
1	-1.219(-10)	5.019(-08)	8.487(-05)	-8.316(-02)	-1.089(1)
2	-3.058(-10)	4.123(-07)	-1.594(-04)	-1.947(-02)	-1.100(1)
3	-3.924(-10)	5.064(-07)	-1.949(-04)	-1.367(-02)	-7.624(0)
4	3.235(-10)	-3.118(-07)	9.487(-05)	-4.654(-02)	-4.848(0)
5	1.089(-10)	-1.175(-07)	4.661(-05)	-4.435(-02)	-3.236(0)
6	1.933(-11)	-1.262(-08)	1.497(-05)	-4.587(-02)	-1.673(0)
7	3.182(-11)	-2.660(-08)	2.772(-05)	-5.176(-02)	-6.649(-01)
8	-1.294(-10)	1.456(-07)	-2.848(-05)	-4.789(-02)	1.692(-01)
9	-5.541(-11)	1.161(-07)	-3.996(-05)	-4.513(-02)	1.195(0)
10	-1.056(-10)	1.804(-07)	-6.526(-05)	-4.296(-02)	1.756(0)

* Reference: NARF-61-39T, "Shield Penetration Programs C-17 and L-63", D. M. Peterson, General Dynamics, Fort Worth, December 1961

** Numbers in parenthesis refer to powers of 10.

TABLE 3-11

EXTRAPOLATION PARAMETERS FOR CARBON MONOVARIANT DATA

Neutron Group No.	λ
1	0.0273
2	0.0245
3	0.0270
4	0.0282
5	0.0305
6	0.0322
7	0.0332
8	0.0332
9	0.0332
10	0.0332

TABLE 3-12

KAP-V GAMMA RAY AND NEUTRON RESPONSE DATA

	GAMMA				NEUTRON						
	Rads (C)/Hr	Btu/in^3-sec H (ρ = 0.07 g/cm^3)	Btu/in^3-sec CH_2 (ρ = 0.14 g/cm^3)	Btu/in^3-sec CH_2 (ρ = 0.59 g/cm^3)	Rads (Ethylene) / Hour	Differential Number Flux (n/cm^2 - sec - Mev)	Total Flux E > 1.5 Mev (n / cm^2 - sec)	Total Flux E > 2.9 Mev (n / cm^2 - sec)	Btu/in^3-Sec H (ρ = 0.07 g/cm^3)	Btu/in^3 - sec CH_2 (ρ = 0.14 g/cm^3)	Btu/in^3-sec CH_2 (ρ = 0.59 g/cm^3)
1	8.5 (-7)	4.44 (-18)	5.714 (-18)	2.408 (-17)	1.16 (-4)	1.0	4.0	4.0	2.041 (-15)	7.058 (-16)	2.9748 (-15)
2	8.8 (-7)	4.616 (-18)	5.868 (-18)	2.473 (-17)	1.14 (-4)	1.0	4.0	4.0	2.115 (-15)	6.867 (-16)	2.894 (-15)
3	9.2 (-7)	4.892 (-18)	6.132 (-18)	2.584 (-17)	8.01 (-5)	1.0	3.0	3.0	1.462 (-15)	4.543 (-16)	1.914 (-15)
4	9.5 (-7)	5.293 (-18)	6.527 (-18)	2.751 (-17)	5.2 (-5)	1.0	2.0	2.0	0.9269 (-15)	2.981 (-16)	1.256 (-15)
5	1.05 (-6)	5.894 (-18)	7.129 (-18)	3.004 (-17)	4.6 (-5)	1.0	2.0	2.0	0.9008 (-15)	2.815 (-16)	1.186 (-15)
6	1.15 (-6)	6.614 (-18)	7.855 (-18)	3.31 (-17)	3.3 (-5)	1.0	1.5	1.5	0.5712 (-15)	1.883 (-16)	7.936 (-15)
7	1.23 (-6)	7.218 (-18)	8.463 (-18)	3.567 (-17)	1.9 (-5)	1.0	1.0	0.5	0.3612 (-15)	1.157 (-16)	4.878 (-16)
8	1.27 (-6)	7.643 (-18)	8.891 (-18)	3.747 (-17)	1.58 (-5)	1.0	1.0	0.0	0.3057 (-15)	0.9574 (-16)	4.034 (-16)
9	1.37 (-6)	8.207 (-18)	9.472 (-18)	3.992 (-17)	9.48 (-6)	1.0	0.0	0.0	0.1840 (-15)	0.5708 (-16)	2.405 (-16)
10	1.48 (-6)	8.845 (-18)	1.020 (-17)	4.30 (-17)	3.39 (-6)	1.0	0.0	0.0	0.08175 (-15)	0.2495 (-16)	1.051 (-16)
11	1.61 (-6)	9.371 (-18)	1.082 (-17)	4.564 (-17)							
12	1.67 (-6)	1.021 (-17)	1.167 (-17)	4.929 (-17)							
13	1.66 (-6)	9.929 (-18)	1.137 (-17)	4.792 (-17)							

code. These data are shown in Table 3-11. These data were obtained from the slope of the carbon moments data for each group.

Response Data

The final set of data which was provided to the KAP-V code was the response data as shown in Table 3-12. These data are for the thirteen gamma ray groups and 10 neutron energy points used in KAP-V. All neutron response data includes the energy band width in order to provide the proper response data.

In the review of the data provided in the MSFC code package in relation to the current experiment analysis, one error was noted in the response functions and this error has been corrected in the present analysis. The error which was in the previous code package data was in the neutron response function data. In the KAP-V code the differential neutron spectra calculational methods to provide differential number spectra of neutrons, requires the entry of response functions which include the energy band width of each particular energy group in the differential spectrum in order to provide total number of particles. The error in the previous data occurred when the response data was not multiplied by ΔE. The correction has been made in the present KAP-V analysis and the response functions are presented in Table 3-12.

In summary, the KAP-V calculations were carried out for the complete detector location map as shown in Section 4. A total of 25 detectors were calculated for configuration 4B and because of the computer time involved in running configuration 7D calculations, a total of 16 detectors were run as shown in Table 4-1. These data provided a fairly complete map of the calculated data within the tank and provided sufficient detail to plot radial traverses.

A complete listing of the KAP-V problems 4B and 7D is included in the Appendix and the reader is referred to these listings for the entry of geometrical description data in KAP-V.

4. RESULTS OF ANALYSIS

Selected calculated neutron and gamma radiation levels in the propellant tank hydrogen simulation are presented in this section in tabular form to illustrate these data in some detail. A portion of these data and additional data are presented graphically in Sections 5 and 6. Figure 4-1 shows a detector coordinate grid superimposed upon the propellant tank. This grid defines the locations of the detector points used in the KAP-V and FASTER analyses. The scale on the left hand side of Figure 4-1 gives dimensions (in centimeters) from the bottom of the tank hemisphere. The scale on the right hand side of the figure shows distances in centimeters from the dome (aft) end of the PAX-E5 core. The detector horizontal traverses were selected to coincide with the positions of the traversing tubes located in the MSFC tank.

Table 4-1 indicates which of the detectors were used in the various KAP-V and FASTER calculations. The KAP-V calculations for Configuration 4B were made at all 25 detector points. However, for Configuration 7D calculations, only 16 of the detectors were used because of the limited amount of experimental data available. Eight detector locations were employed in the FASTER calculation of the neutron radiation levels for Configuration 4B. Five detector locations were employed in the FASTER calculations of gamma ray levels for configuration 4B and 7D. Fewer detectors were used in the FASTER calculation than the point kernel calculation because of the greater cost of the Monte Carlo calculations.

4.1 FASTER ANALYSIS

The results of the FASTER calculations of the neutron radiation levels for Configuration 4B are presented in Table 4-2 for eight detector locations. The following type of response data are presented: the first column presents the fast neutron flux for neutrons with energies greater than 2.9 Mev; the second column presents fast neutron flux greater than 1.5 Mev. The third column presents the fast neutron dose rate in tissue rads/hour. The fourth column presents the associated relative statistical error. Fast neutron dose

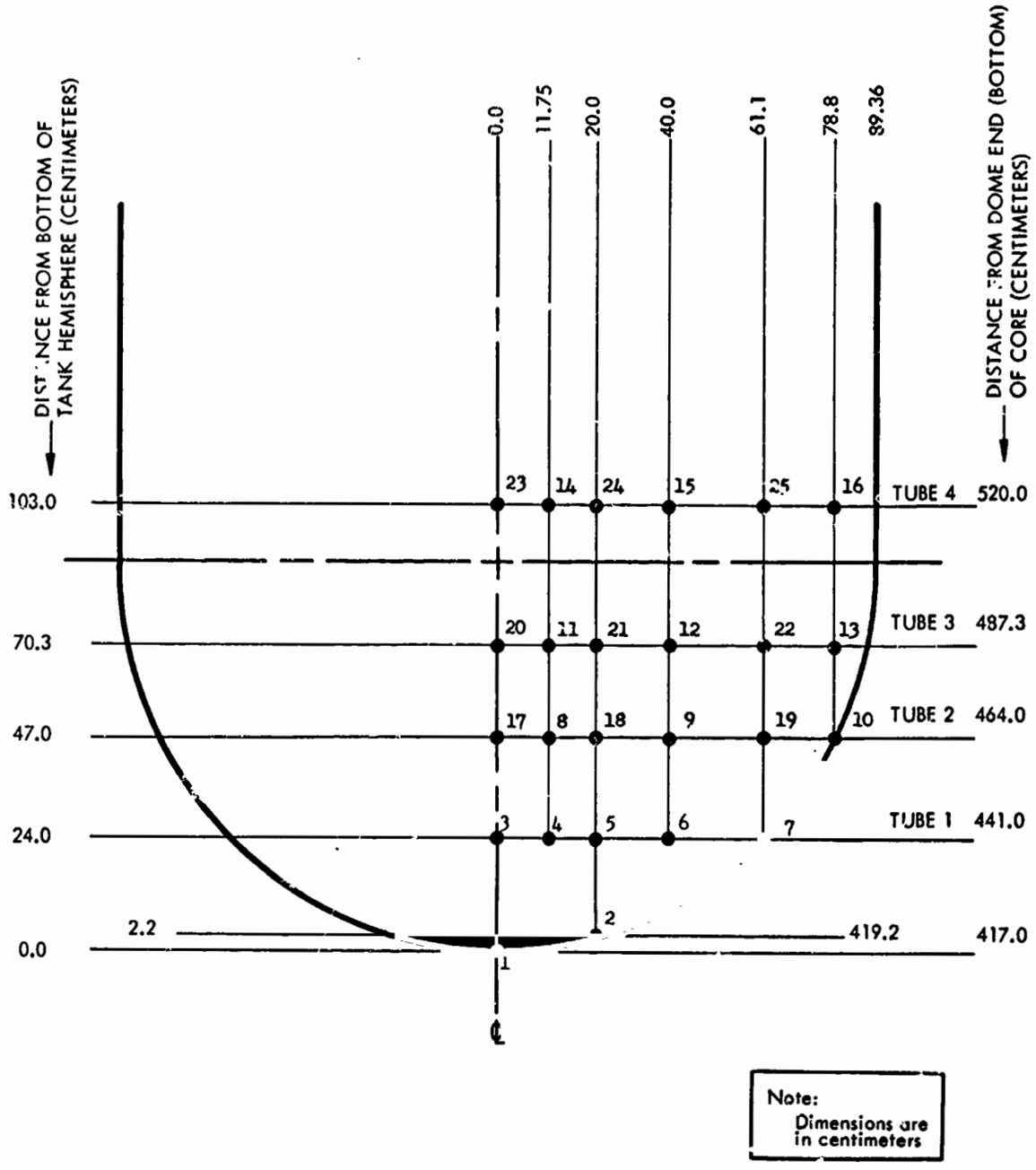

Figure 4-1. Detector Coordinates for KAP-V, FASTER
(Note: Only Selected Points Were Run According to Table 4.1)

TABLE 4-1

DETECTOR LOCATIONS IN KAP-V AND FASTER PROBLEMS

	KAP-V		FASTER				
			4B	4B&7D			
Number	7D	4B	Neutron	Gamma	X(cm)	Y(cm)	Z(cm)
1	X	X	X	X	0.0	0.0	417.0
2		X			20.0	0.0	419.2
3	X	X			0.0	0.0	441.0
4	X	X	X	X	11.75	0.0	441.0
5	X	X			20.0	0.0	441.0
6	X	X	X		40.0	0.0	441.0
7	X	X			61.0	0.0	441.0
8	X	X	X	X	11.75	0.0	464.0
9		X			40.0	0.0	464.0
10		X			78.8	0.0	464.0
11	X	X	X	X	11.75	0.0	487.3
12	X	X			40.0	0.0	487.3
13	X	X	X		78.8	0.0	487.3
14	X	X	X	X	11.75	0.0	520.0
15		X			40.0	0.0	520.0
16		X			78.8	0.0	520.0
17		X			0.0	0.0	464.0
18		X			20.0	0.0	464.0
19		X	X		61.1	0.0	464.0
20	X	X			0.0	0.0	487.3
21	X	X			20.0	0.0	487.3
22	X	X			61.1	0.0	487.3
23		X			0.0	0.0	520.0
24		X			20.0	0.0	520.0
25		X			61.1	0.0	520.0

Astronuclear Laboratory

TABLE 4-2

FASTER NEUTRON RESULTS AS A FUNCTION OF PACKET AND RESPONSE FUNCTION FOR CONFIGURATION 4B

Detector	1		2		3		4		5		6		7		8		9		10		Detector Coordinates X	Y	Z
	$\phi > 2.9$ Mev Neutrons/cm^2-sec		$\phi > 1.5$ Mev Neutrons/cm^2-sec		Rads (Tissue)/Hr		Relative Error		Rads (Ethylene)/Hr		Relative Error		REM/Hr		Relative Error		Btu/in^3-Sec (Hydrogen)		Relative Error				
																					0	0	4.17 (+2)
100	6.66	(+1)	3.25	(+2)	5.97	(-3)	2.29	(-1)	8.37	(-3)	2.92	(-1)	5.48	(-2)	3.08	(-1)	2.18	(-13)	2.92	(-1)			
200	7.60	(+1)	4.09	(+2)	7.68	(-3)	2.23	(-1)	1.07	(-2)	2.24	(-1)	7.08	(-2)	2.33	(-1)	2.80	(-13)	2.24	(-1)			
300	7.63	(+1)	4.10	(+2)	7.85	(-3)	1.74	(-1)	1.10	(-2)	1.74	(-1)	7.27	(-2)	1.80	(-1)	2.87	(-13)	1.73	(-1)			
400	7.88	(+1)	4.27	(+2)	8.23	(-3)	1.42	(-1)	1.15	(-2)	1.43	(-1)	7.63	(-2)	1.47	(-1)	3.01	(-13)	1.43	(-1)			
500	7.85	(+1)	4.29	(+2)	8.09	(-3)	1.27	(-1)	1.12	(-2)	1.27	(-1)	7.45	(-2)	1.31	(-1)	2.94	(-13)	1.28	(-1)			
600	8.59	(+1)	4.48	(+2)	8.24	(-3)	1.14	(-1)	1.19	(-2)	1.14	(-1)	7.58	(-2)	1.17	(-1)	3.01	(-13)	1.15	(-1)			
700	8.42	(+1)	4.31	(+2)	7.97	(-3)	1.15	(-1)	1.11	(-2)	1.15	(-1)	7.33	(-2)	1.18	(-1)	2.91	(-13)	1.15	(-1)			
800	8.45	(+1)	4.24	(+2)	7.73	(-3)	1.05	(-1)	1.06	(-2)	1.06	(-1)	7.09	(-2)	1.09	(-1)	2.82	(-13)	1.06	(-1)			
Detector 4																							
100	9.22	(0)	1.66	(+1)	3.79	(-4)	3.88	(-1)	5.40	(-4)	3.91	(-1)	3.16	(-3)	4.19	(-1)	1.38	(-14)	3.92	(-1)	1.17	(+1) 0.0	4.41 (+2)
200	9.90	(0)	1.97	(+1)	3.61	(-4)	2.77	(-1)	9.12	(-4)	2.78	(-1)	2.97	(-3)	3.00	(-1)	1.31	(-14)	2.80	(-1)			
300	1.13	(+1)	2.42	(+1)	4.81	(-4)	2.87	(-1)	6.81	(-4)	2.88	(-1)	4.02	(-3)	3.08	(-1)	1.75	(-14)	2.91	(-1)			
400	1.12	(+1)	2.31	(+1)	4.50	(-4)	2.40	(-1)	6.37	(-4)	2.41	(-1)	3.73	(-3)	2.58	(-1)	1.66	(-14)	2.44	(-1)			
500	1.04	(+1)	2.22	(+1)	4.57	(-4)	2.31	(-1)	6.47	(-4)	2.31	(-1)	3.86	(-3)	2.49	(-1)	1.67	(-14)	2.34	(-1)			
600	1.03	(+1)	2.23	(+1)	4.34	(-4)	2.08	(-1)	6.15	(-4)	2.09	(-1)	3.65	(-3)	2.26	(-1)	1.58	(-14)	2.11	(-1)			
700	1.07	(+1)	2.25	(+1)	4.30	(-4)	1.86	(-1)	6.06	(-4)	1.87	(-1)	3.60	(-3)	2.03	(-1)	1.56	(-14)	1.89	(-1)			
800	1.17	(+1)	2.52	(+1)	4.59	(-4)	2.08	(-1)	6.48	(-4)	2.08	(-1)	3.84	(-3)	2.22	(-1)	1.66	(-14)	2.10	(-1)			
Detector 8																							
100	3.19	(0)	5.26	(0)	8.20	(-5)	3.39	(-1)	1.15	(-4)	3.37	(-1)	6.26	(-4)	3.51	(-1)	2.94	(-15)	3.39	(-1)	1.17	(+1) 0.0	4.44 (+2)
200	2.41	(0)	3.95	(0)	6.11	(-5)	2.42	(-1)	8.63	(-5)	2.40	(-1)	4.64	(-4)	2.54	(-1)	2.19	(-15)	2.42	(-1)			
300	2.32	(0)	4.06	(0)	6.23	(-5)	2.18	(-1)	8.81	(-5)	2.17	(-1)	4.78	(-4)	2.29	(-1)	2.24	(-15)	2.19	(-1)			
400	2.32	(0)	3.89	(0)	5.96	(-5)	1.86	(-1)	8.42	(-5)	1.86	(-1)	4.53	(-4)	1.96	(-1)	2.14	(-15)	1.87	(-1)			
500	2.17	(0)	3.58	(0)	5.64	(-5)	1.65	(-1)	7.98	(-5)	1.64	(-1)	4.31	(-4)	1.74	(-1)	2.03	(-15)	1.66	(-1)			
600	2.02	(0)	3.30	(0)	5.19	(-5)	1.48	(-1)	7.34	(-5)	1.48	(-1)	3.96	(-4)	1.56	(-1)	1.87	(-15)	1.49	(-1)			
700	1.87	(0)	3.02	(0)	4.77	(-5)	1.38	(-1)	6.76	(-5)	1.38	(-1)	3.63	(-4)	1.46	(-1)	1.72	(-15)	1.39	(-1)			
800	1.81	(0)	2.91	(0)	4.61	(-5)	1.28	(-1)	6.53	(-5)	1.28	(-1)	3.50	(-4)	1.36	(-1)	1.66	(-15)	1.29	(-1)			
Detector 11																							
100	2.81	(-1)	4.62	(-1)	7.01	(-6)	3.25	(-1)	9.95	(-6)	3.23	(-1)	5.24	(-5)	3.34	(-1)	2.55	(-16)	3.25	(-1)	1.17	(+1) 0.0	4.87 (+2)
200	2.79	(-1)	4.21	(-1)	6.61	(-6)	2.31	(-1)	9.40	(-6)	2.29	(-1)	4.92	(-5)	2.45	(-5)	2.39	(-16)	2.31	(-1)			
300	2.93	(-1)	4.61	(-1)	7.49	(-6)	2.59	(-1)	1.06	(-5)	2.55	(-1)	5.71	(-5)	2.88	(-1)	2.71	(-16)	2.59	(-1)			
400	2.92	(-1)	4.45	(-1)	7.30	(-6)	2.13	(-1)	1.03	(-5)	2.10	(-1)	5.52	(-5)	2.38	(-1)	2.64	(-16)	2.13	(-1)			
500	4.21	(-1)	9.32	(-1)	1.73	(-5)	6.04	(-1)	2.46	(-5)	6.03	(-1)	1.44	(-4)	6.43	(-1)	6.53	(-16)	6.07	(-1)			
600	4.17	(-1)	8.58	(-1)	1.57	(-5)	5.59	(-1)	2.23	(-5)	5.58	(-1)	1.29	(-4)	6.01	(-1)	5.73	(-16)	5.62	(-1)			
700	3.84	(-1)	7.66	(-1)	1.39	(-5)	5.30	(-1)	1.98	(-5)	5.29	(-1)	1.14	(-4)	5.74	(-1)	5.09	(-16)	5.33	(-1)			
800	3.62	(-1)	7.03	(-1)	1.29	(-5)	5.01	(-1)	1.83	(-5)	5.00	(-1)	1.05	(-4)	5.44	(-1)	4.71	(-16)	5.04	(-1)			
Detector 14																							
100	1.98	(-2)	6.40	(-2)	9.19	(-7)	6.86	(-1)	1.28	(-6)	6.79	(-1)	7.87	(-6)	7.32	(-1)	3.33	(-17)	6.84	(-1)	1.17	(+1) 0.0	5.2 (+2)
200	2.73	(-2)	5.32	(-2)	8.08	(-7)	4.68	(-1)	1.14	(-6)	4.62	(-1)	6.39	(-6)	5.20	(-1)	2.92	(-17)	4.67	(-1)			
300	2.61	(-2)	4.57	(-2)	7.06	(-7)	3.88	(-1)	1.00	(-6)	3.82	(-1)	5.45	(-6)	4.39	(-1)	2.57	(-17)	3.8.	(-1)			
400	2.24	(-2)	3.74	(-2)	5.83	(-7)	3.47	(-1)	8.28	(-7)	3.14	(-1)	4.45	(-6)	3.96	(-1)	2.12	(-17)	3.46	(-1)			
500	2.09	(-2)	3.36	(-2)	5.32	(-7)	3.08	(-1)	7.58	(-7)	3.02	(-1)	4.03	(-6)	3.53	(-1)	1.94	(-17)	3.06	(-1)			
600	2.64	(-2)	4.09	(-2)	6.51	(-7)	2.94	(-1)	9.28	(-7)	2.90	(-1)	4.89	(-6)	3.26	(-1)	2.37	(-17)	2.93	(-1)			
700	2.51	(-2)	3.75	(-2)	6.10	(-7)	2.69	(-1)	8.71	(-7)	2.65	(-1)	4.56	(-6)	2.98	(-1)	2.22	(-17)	2.68	(-1)			
800	2.76	(-2)	4.15	(-2)	6.83	(-7)	2.54	(-1)	9.72	(-7)	2.51	(-1)	5.15	(-6)	2.79	(-1)	2.48	(-17)	2.53	(-1)			
Detector 6																							
100	1.74	(+1)	4.64	(+1)	9.14	(-4)	4.48	(-1)	1.29	(-3)	4.49	(-1)	7.94	(-3)	4.70	(-1)	3.31	(-14)	4.50	(-1)	4.0	(+1) 0.0	4.41 (+2)
200	1.94	(+1)	4.85	(+1)	8.76	(-4)	2.77	(-1)	1.23	(-3)	2.78	(-1)	7.48	(-3)	2.93	(-1)	3.18	(-14)	2.79	(-1)			
300	2.02	(+1)	5.47	(+1)	1.34	(-3)	4.18	(-1)	1.90	(-3)	4.20	(-1)	1.19	(-2)	4.42	(-1)	4.95	(-14)	4.24	(-1)			
400	1.97	(+1)	5.72	(+1)	1.58	(-3)	4.11	(-1)	2.23	(-3)	4.12	(-1)	1.44	(-2)	4.34	(-1)	5.80	(-14)	4.15	(-1)			
500	1.90	(+1)	5.42	(+1)	1.44	(-3)	3.65	(-1)	2.03	(-3)	3.65	(-1)	1.31	(-2)	3.87	(-1)	5.29	(-14)	3.68	(-1)			
600	1.86	(+1)	5.10	(+1)	1.29	(-3)	3.37	(-1)	1.83	(-3)	3.38	(-1)	1.17	(-2)	3.60	(-1)	4.75	(-14)	3.41	(-1)			
700	1.89	(+1)	5.02	(+1)	1.22	(-3)	3.10	(-1)	1.73	(-3)	3.11	(-1)	1.10	(-2)	3.33	(-1)	4.49	(-14)	3.14	(-1)			
800	1.92	(+1)	5.11	(+1)	1.19	(-3)	2.86	(-1)	1.68	(-3)	2.87	(-1)	1.04	(-2)	3.09	(-1)	4.37	(-14)	2.90	(-1)			
Detector 19																							
100	7.92	(0)	1.62	(+1)	2.79	(-4)	3.65	(-1)	3.94	(-4)	3.64	(-1)	2.30	(-3)	3.94	(-1)	1.01	(-14)	3.68	(-1)	6.10	(+1) 0.0	4.64 (+2)
200	7.47	(0)	1.77	(+1)	3.03	(-4)	3.06	(-1)	4.27	(-4)	3.05	(-1)	2.55	(-3)	3.31	(-1)	1.10	(-14)	3.08	(-1)			
300	7.02	(0)	2.09	(+1)	3.32	(-4)	3.37	(-1)	4.65	(-4)	3.35	(-1)	2.87	(-3)	3.62	(-1)	1.20	(-14)	3.39	(-1)			
400	7.21	(0)	2.00	(+1)	3.15	(-4)	2.81	(-1)	4.41	(-4)	2.79	(-1)	2.69	(-3)	3.04	(-1)	1.14	(-14)	2.83	(-1)			
500	6.8	(0)	1.78	(+1)	2.82	(-4)	2.50	(-1)	3.96	(-4)	2.48	(-1)	2.39	(-3)	2.70	(-1)	1.02	(-14)	2.51	(-1)			
600	6.43	(0)	1.59	(+1)	2.53	(-4)	2.33	(-1)	3.55	(-4)	2.31	(-1)	2.12	(-3)	2.53	(-1)	9.15	(-15)	2.34	(-1)			
700	6.19	(0)	1.45	(+1)	2.30	(-4)	2.1.	(-1)	3.23	(-4)	2.14	(-1)	1.91	(-3)	2.37	(-1)	8.32	(-15)	2.18	(-1)			
800	6.18	(0)	1.41	(+1)	2.26	(-4)	1.98	(-1)	3.18	(-4)	1.96	(-1)	1.87	(-3)	2.17	(-1)	8.18	(-15)	1.99	(-1)			
Detector 13																							
100	3.04	(0)	5.15	(0)	8.05	(-5)	2.64	(-1)	1.13	(-4)	2.62	(-1)	6.16	(-4)	2.68	(-1)	2.90	(-15)	2.63	(-1)	7.08	(+1) 0.0	4.87 (+2)
200	2.70	(0)	4.61	(0)	7.26	(-5)	1.95	(-1)	1.02	(-4)	1.93	(-1)	5.61	(-4)	2.04	(-1)	2.62	(-15)	1.94	(-1)			
300	3.67	(0)	6.53	(0)	1.01	(-4)	2.27	(-1)	1.44	(-4)	2.25	(-1)	7.96	(-4)	2.36	(-1)	3.67	(-15)	2.26	(-1)			
400	3.43	(0)	5.91	(0)	9.50	(-5)	1.95	(-1)	1.34	(-4)	1.94	(-1)	7.40	(-4)	2.04	(-1)	3.42	(-15)	1.95	(-1)			
500	3.20	(0)	5.39	(0)	8.71	(-5)	1.75	(-1)	1.20	(-4)	1.74	(-1)	6.76	(-4)	1.84	(-1)	3.14	(-15)	1.75	(-1)			
600	2.98	(0)	4.89	(0)	7.91	(-5)	1.61	(-1)	1.12	(-4)	1.60	(-1)	6.10	(-4)	1.70	(-1)	2.85	(-15)	1.61	(-1)			
700	2.82	(0)	4.57	(0)	7.40	(-5)	1.47	(-1)	1.04	(-4)	1.45	(-1)	5.68	(-4)	1.55	(-1)	2.67	(-15)	1.47	(-1)			
800	2.82	(0)	4.64	(0)	7.50	(-5)	1.34	(-1)	1.06	(-4)	1.34	(-1)	5.78	(-4)	1.42	(-1)	2.71	(-15)	1.34	(-1)			

NOTE: RADIATION LEVELS ARE PRESENTED PER WATT OF REACTOR POWER

rate in ethylene rads/hour is presented in Column 5 with the associated relative error presented in Column 6. The seventh column presents fast neutron dose rate in units of Rem/hour with the associated relative error presented in Column 8. Columns 9 and 10 present the heating rate in high density polyethylene and the associated relative error. The final three columns present the detector coordinates in centimeters. For each detector, intermediate results are presented after each 100 packets were processed in FASTER. A total of 800 packets were run for the neutron problem. By tabulating the intermediate results after each 100 packets, it is possible to determine whether the answer has stabilized; and by tabulating the relative error after each 100 packets, one can determine whether the error is decreasing in a satisfactory manner; i.e., roughly proportional to the square root of the number of packets run. The relative errors of the tissue rads dose rate is of the order of 10 to 30 percent for all detectors with the exception of Detector 11. The results reported for Detector 11 indicate the need for close inspection of FASTER results and sufficient number of packets to provide convergence. For example, the tissue dose rate appears to have stabilized at a value of approximately 7×10^{-6} with a relative error of 21 percent after only 400 packets. However, between the 400 and 500 packets, a "blow up" occurred. After the 500th packet, the answer has increased by a factor of 2.5 and the relative error increased by a factor of three. Subsequently the "answer" and relative error decreased in magnitude. Thus it appears that the "answer" has not stabilized and that even after 800 packets the relative error is still unreasonably large.

In the case of the FASTER neutron results for Detector 11, an additional FASTER problem was run. Since the 800 packet results suggest that the poor statistics and the unstabilized responses for Detector No. 11 can be associated with the location of that particular detector point, this FASTER neutron problem was rerun for a total of 1500 packets with the position of Detector No. 11 moved 2 cm in the + X direction (redesignated as Detector 11A). The calculated neutron response (tissue rads) for this additional FASTER run is presented in Table 4-3. The result of this additional neutron calculation is about 45 percent less at 800 packets and 60 percent less at 1500 packets than the corresponding data at 800 packets presented in Table 4-2. The new tissue dose rate at 1500 packets agrees with the measured data to within 10 percent. The relative error associated with the tissue dose at

TABLE 4-3

ADDITIONAL FASTER CALCULATIONS OF THE FAST NEUTRON DOSE RATE, DETECTOR NO 11A, CONFIGURATION 4B, HIGH DENSITY POLYETHYLENE

No. of Packets	Rads (Tissue) / Hr - wati	Relative Error
50	6.63 (-6)	3.08 (-1)
100	6.05 (-6)	2.68 (-1)
150	4.92 (-6)	2.17 (-1)
200	7.30 (-6)	3.78 (-1)
250	1.25 (-5)	5.07 (-1)
300	1.17 (-5)	4.62 (-1)
350	1.11 (-5)	4.26 (-1)
400	1.09 (-5)	3.96 (-1)
450	1.02 (-5)	3.74 (-1)
500	1.03 (-5)	3.64 (-1)
550	9.82 (-6)	3.51 (-1)
600	1.03 (-5)	3.34 (-1)
650	9.80 (-6)	3.22 (-1)
700	9.36 (-6)	3.12 (-1)
750	9.17 (-6)	2.99 (-1)
800	8.95 (-6)	2.95 (-1)
850	8.74 (-6)	2.82 (-1)
900	9.04 (-6)	2.68 (-1)
950	9.25 (-6)	2.53 (-1)
1000	8.93 (-6)	2.48 (-1)
1050	8.77 (-6)	2.39 (-1)
1100	8.69 (-6)	2.31 (-1)
1150	8.66 (-6)	2.24 (-1)
1200	8.66 (-6)	2.16 (-1)
1250	8.50 (-6)	2.10 (-1)
1300	8.39 (-6)	2.04 (-1)
1350	8.21 (-6)	2.00 (-1)
1400	8.13 (-6)	1.94 (-1)
1450	7.95 (-6)	1.91 (-1)
1500	7.76 (-6)	1.89 (-1)

Detector No 11A Coordinates

X = 13.75

Y = 0.0

Z = 487.3

800 packets is 30 percent. This comparison indicates that the technique of moving the detector by a small amount resulted in a more rapid stabilization of the "answer." Following the 250 packet intermediate result, the relative error decreases continuously from a value of 51 percent after 250 packets to a value of 19 percent after 1500 packets.

Table 4-4 presents the FASTER code calculations of the gamma ray dose rates and gamma heating rates in the high density polyethylene for Configuration 4B. The format of Table 4-4 is similar to that employed in the previous table. Four types of photon responses are presented: (1) gamma ray dose rate in carbon rads/hour, (2) gamma ray dose rate in tissue rads/hour, (3) heating rate in BTU/cubic inch-second in liquid hydrogen, (4) heating rates in BTU/cubic inch-second in polyethylene having the density equal to that in the experiment. Included in Table 4-4 are the associated relative errors which apply to the dose rate and heating rate responses. The gamma ray response data are also presented after each 100 packets. A total of 1000 packets was run in the gamma problem for Configuration 4B. The relative error is 12 to 18 percent for each detector with the exception of Detector No. 11. The behavior of the intermediate dose rates (tissue rads) for Detector 11 provides another example of the need for closely examining intermediate results. The intermediate results after 100, 200, and 300 packets appear to be converged and to have a relatively low (24 percent) statistical uncertainty. However, after 400 packets, there is an increase in the answer with accompanying reduction in the statistical accuracy. The answer decreases slowly with an accompanying decrease in the magnitude of the relative error after 700 packets have been run. There is then another increase in the magnitude of the dose rate response after 800 packets and again the statistical accuracy has decreased. It appears from the last three intermediate responses that the FASTER result has not stabilized.

The results of the FASTER gamma calculations for Configuration 7D with low density hydrogen simulation in the MSFC tank are presented in Table 4-5. The format and the response data are identical to that in Table 4-2. In general, the relative statistical errors associated with the response data for Configuration 7D are larger than were observed for Configuration 4B. For 7D the relative errors vary between 25 and 36 percent. These larger errors are attributed to the greater mass of material between the reactor and the

Astronuclear Laboratory

TABLE 4-4
FASTER GAMMA RESULTS AS A FUNCTION OF PACKET AND RESPONSE FUNCTION FOR CONFIGURATION 4B

	Rads (Carbon)/Hr	Relative Error	Rads (Tissue)/Hr	Relative Error	BTU/sec $in^3(LH_2)$	Relative Error	BTU/sec $in^3(CH_2)$	Relative Error	Detector Coordinates		
Detector 1	1	2	3	4	5	6	7	8	X	Y	Z
100	1.14 (-2)	3.14 (-1)	1.20 (-2)	3.14 (-1)	6.55 (-14)	3.17 (-1)	3.28	(-13) 3.15 (-1)	0.0	0.0	4.17 (+2)
200	1.13 (-2)	2.24 (-1)	1.18 (-2)	2.24 (-1)	6.53 (-14)	2.26 (-1)	3.26	(-13) 2.25 (-1)			
300	9.95 (-3)	1.83 (-1)	1.04 (-2)	1.84 (-1)	5.72 (-14)	1.85 (-1)	2.86	(-13) 1.84 (-1)			
400	1.07 (-2)	1.59 (-1)	1.12 (-2)	1.59 (-1)	6.18 (-14)	1.60 (-1)	3.09	(-13) 1.59 (-1)			
500	9.90 (-3)	1.42 (-1)	1.03 (-2)	1.42 (-1)	5.69 (-14)	1.43 (-1)	2.84	(-13) 1.42 (-1)			
600	1.08 (-2)	1.63 (-1)	1.14 (-2)	1.64 (-1)	6.27 (-14)	1.66 (-1)	3.12	(-13) 1.63 (-1)			
700	1.05 (-2)	1.47 (-1)	1.11 (-2)	1.48 (-1)	6.10 (-14)	1.50 (-1)	3.04	(-13) 1.47 (-1)			
800	1.01 (-2)	1.36 (-1)	1.07 (-2)	1.37 (-1)	5.87 (-14)	1.39 (-1)	2.92	(-13) 1.37 (-1)			
900	9.73 (-3)	1.28 (-1)	1.02 (-2)	1.29 (-1)	5.60 (-14)	1.31 (-1)	2.79	(-13) 1.28 (-1)			
1000	9.46 (-3)	1.20 (-1)	9.96 (-3)	1.20 (-1)	5.44 (-14)	1.22 (-1)	2.71	(-13) 1.20 (-1)			
Detector 4											
100	7.70 (-3)	4.60 (-1)	8.23 (-3)	4.61 (-1)	4.48 (-14)	4.66 (-1)	2.21	(-13) 4.61 (-1)	1.17 (+1)	0.0	4.41 (+2)
200	6.33 (-3)	3.18 (-1)	6.77 (-3)	3.19 (-1)	3.66 (-14)	3.23 (-1)	1.82	(-13) 3.18 (-1)			
300	7.62 (-3)	2.61 (-1)	8.35 (-3)	2.71 (-1)	4.40 (-14)	2.63 (-1)	2.19	(-13) 2.61 (-1)			
400	7.54 (-3)	2.20 (-1)	8.19 (-3)	2.29 (-1)	4.35 (-14)	2.22 (-1)	2.16	(-13) 2.20 (-1)			
500	6.85 (-3)	2.00 (-1)	7.41 (-3)	2.08 (-1)	3.95 (-14)	2.02 (-1)	1.96	(-13) 2.00 (-1)			
600	6.96 (-3)	2.06 (-1)	7.56 (-3)	2.14 (-1)	4.02 (-14)	2.08 (-1)	2.00	(-13) 2.06 (-1)			
700	6.55 (-3)	1.93 (-1)	7.10 (-3)	2.01 (-1)	3.78 (-14)	1.96 (-1)	1.88	(-13) 1.94 (-1)			
800	6.44 (-3)	1.83 (-1)	6.97 (-3)	1.90 (-1)	3.72 (-14)	1.85 (-1)	1.85	(-13) 1.83 (-1)			
900	6.26 (-3)	1.71 (-1)	6.77 (-3)	1.78 (-1)	3.61 (-14)	1.74 (-1)	1.80	(-13) 1.72 (-1)			
1000	6.40 (-3)	1.59 (-1)	6.94 (-3)	1.66 (-1)	3.68 (-14)	1.61 (-1)	1.83	(-13) 1.60 (-1)			
Detector 8											
100	3.63 (-3)	4.28 (-1)	4.01 (-3)	4.35 (-1)	2.07 (-14)	4.34 (-1)	1.04	(-13) 4.29 (-1)	1.17 (+1)	0.0	4.64 (+2)
200	4.61 (-3)	3.48 (-1)	5.06 (-3)	3.52 (-1)	2.66 (-14)	3.54 (-1)	1.32	(-13) 3.49 (-1)			
300	4.21 (-3)	3.15 (-1)	4.89 (-3)	3.53 (-1)	2.36 (-14)	3.07 (-1)	1.20	(-13) 3.13 (-1)			
400	3.98 (-3)	2.61 (-1)	4.59 (-3)	2.92 (-1)	2.24 (-14)	2.54 (-1)	1.13	(-13) 2.59 (-1)			
500	4.54 (-3)	2.62 (-1)	5.15 (-3)	2.81 (-1)	2.59 (-14)	2.60 (-1)	1.30	(-13) 2.61 (-1)			
600	4.11 (-4)	2.39 (-1)	4.63 (-3)	2.58 (-1)	2.34 (-14)	2.38 (-1)	1.17	(-13) 2.38 (-1)			
700	3.93 (-3)	2.20 (-1)	4.41 (-3)	2.38 (-1)	2.24 (-14)	2.19 (-1)	1.12	(-13) 2.19 (-1)			
800	3.76 (-3)	2.04 (-1)	4.20 (-3)	2.21 (-1)	2.14 (-14)	2.03 (-1)	1.07	(-13) 2.04 (-1)			
900	3.54 (-3)	1.94 (-1)	3.94 (-3)	2.10 (-1)	2.01 (-14)	1.93 (-1)	1.01	(-13) 1.93 (-1)			
1000	3.58 (-3)	1.81 (-1)	3.97 (-3)	1.96 (-1)	2.04 (-14)	1.80 (-1)	1.02	(-13) 1.80 (-1)			
Detector 11											
100	1.80 (-3)	3.22 (-1)	1.92 (-3)	3.23 (-1)	1.01 (-14)	3.27 (-1)	5.17	(-14) 3.23 (-1)	1.17 (+1)	0.0	4.87 (+2)
200	1.97 (-3)	2.38 (-1)	2.11 (-3)	2.39 (-1)	1.11 (-14)	2.43 (-1)	5.65	(-14) 2.39 (-1)			
300	1.95 (-3)	2.40 (-1)	2.08 (-3)	2.41 (-1)	1.10 (-14)	2.47 (-1)	5.58	(-14) 2.41 (-1)			
400	2.80 (-3)	4.36 (-1)	3.03 (-3)	4.42 (-1)	1.61 (-14)	4.48 (-1)	8.07	(-14) 4.39 (-1)			
500	2.70 (-3)	3.98 (-1)	2.99 (-3)	4.13 (-1)	1.54 (-14)	4.07 (-1)	7.77	(-14) 4.00 (-1)			
600	2.51 (-3)	3.64 (-1)	2.77 (-3)	3.78 (-1)	1.43 (-14)	3.73 (-1)	7.22	(-14) 3.66 (-1)			
700	2.35 (-3)	3.39 (-1)	2.58 (-3)	3.53 (-1)	1.33 (-14)	3.48 (-1)	6.74	(-14) 3.41 (-1)			
800	3.75 (-3)	5.31 (-1)	4.08 (-3)	5.35 (-1)	2.19 (-14)	5.45 (-1)	1.07	(-13) 5.33 (-1)			
900	3.52 (-3)	5.06 (-1)	3.83 (-3)	5.11 (-1)	2.05 (-14)	5.20 (-1)	1.01	(-13) 5.09 (-1)			
1000	3.27 (-3)	4.86 (-1)	3.56 (-3)	4.90 (-1)	1.90 (-14)	5.00 (-1)	9.41	(-14) 4.88 (-1)			
Detector 14											
100	5.37 (-4)	3.48 (-1)	5.97 (-4)	3.79 (-1)	2.99 (-15)	3.48 (-1)	1.53	(-14) 3.47 (-1)	1.17 (+1)	0.0	5.20 (+2)
200	6.75 (-4)	3.07 (-1)	7.33 (-4)	3.21 (-1)	3.80 (-15)	3.12 (-1)	1.93	(-14) 3.06 (-1)			
300	6.07 (-4)	2.49 (-1)	6.55 (-4)	2.60 (-1)	3.41 (-15)	2.53 (-1)	1.73	(-14) 2.50 (-1)			
400	6.38 (-4)	2.66 (-1)	6.81 (-4)	2.71 (-1)	3.55 (-15)	2.69 (-1)	1.82	(-14) 2.67 (-1)			
500	6.56 (-4)	2.24 (-1)	6.99 (-4)	2.28 (-1)	3.67 (-15)	2.20 (-1)	1.87	(-14) 2.25 (-1)			
600	6.61 (-4)	1.94 (-1)	7.05 (-4)	1.97 (-1)	3.69 (-15)	1.96 (-1)	1.89	(-14) 1.94 (-1)			
700	6.60 (-4)	1.77 (-1)	7.03 (-4)	1.79 (-1)	3.70 (-15)	1.79 (-1)	1.89	(-14) 1.77 (-1)			
800	6.89 (-4)	1.81 (-1)	7.39 (-4)	1.86 (-1)	3.86 (-15)	1.84 (-1)	1.97	(-14) 1.82 (-1)			
900	7.13 (-4)	1.79 (-1)	7.65 (-4)	1.83 (-1)	4.02 (-15)	1.81 (-1)	2.04	(-14) 1.79 (-1)			
1000	7.23 (-4)	1.68 (-1)	7.74 (-4)	1.72 (-1)	4.07 (-15)	1.70 (-1)	2.07	(-14) 1.68 (-1)			

NOTE: RADIATION LEVELS ARE PRESENTED PER WATT OF REACTOR POWER ;

Astronuclear Laboratory

TABLE 4-5
FASTER GAMMA RESULTS AS A FUNCTION OF PACKET AND RESPONSE FUNCTION FOR CONFIGURATION 7D

	Rads (Carbon) Hr	Relative Error	Rads(Tissue) Hr	Relative Error	BTU/sec in^3 (LiH_2)	Relative Error	BTU/sec in^3 (CH_2)	Relative Error	Detector Coordinates		
Detector 1	1	2	3	4	5	6	7	8	X	Y	Z
100	8.61 (-4)	6.80 (-1)	9.18 (-4)	6.88 (-1)	4.91 (-15)	6.89 (-1)	5.87 (-15)	6.82 (-1)	0.0	0.0	4.17 (+2)
200	6.67 -4)	4.80 (-1)	7.02 (-4)	4.88 (-1)	3.77 (-15)	4.87 (-1)	4.51 (-15)	4.82 (-1)			
300	1.15 (-3)	5.18 (-1)	1.20 (-3)	5.18 (-1)	6.61 (-15	5.24 (-1)	7.87 (-15)	5.19 (-1)			
400	1.07 (-3)	4.63 (-1)	1.12 (-3)	4.63 (-1)	6.18 (-15)	4.69 (-1)	7.33 (-15)	4.65 (-1)			
500	1.18 (-3)	4.58 (-1)	1.24 (-3)	4.59 (-1)	6.85 (-15)	4.65 (-1)	8.06 (-15)	4.59 (-1)			
600	1.13 (-3)	4.11 (-1)	1.19 (-3)	4.11 (-1)	6.59 (-15)	4.16 (-1)	7.73 (-15)	4.12 (-1)			
700	1.03 (-3)	3.89 (-1)	1.08 (-3)	3.89 (-1)	5.98 (-15)	3.95 (-1)	7.03 (-15)	3.90 (-1)			
800	9.50 -4)	3.72 (-1)	9.99 (-4	3.72 (-1)	5.50 (-15)	3.77 (-1)	6.47 (-15)	3.73 (-1)			
900	8.94 (-4)	3.53 (-1)	9.40 (-4)	3.53 (-1)	5.17 (-15)	3.58 (-1)	6.09 (-15)	3.53 (-1)			
1000	8.63 (-4)	3.31 (-1)	9.07 (-4	3.31 (-1)	4.98 (-15)	3.37 (-1)	5.88 (-15)	3.32 (-1)			
Detector 4											
100	4.97 (-4)	5.96 (-1)	5.21 (-4)	5.95 (-1)	2.81 (-15)	6.01 (-1)	3.38 (-15)	5.97 (-1)	1.17 (+1)	0.0	4.41 (+2)
200	6.57 (-4)	6.25 (-1)	6.92 (-4)	6.28 (-1)	3.82 (-15)	6.36 (-1)	4.46 (-15)	6.24 (-1)			
300	8.89 (-4)	5.68 (-1)	9.33 (-4)	5.67 (-1)	5.13 (-15)	5.77 (-1)	6.06 (-15)	5.69 (-1)			
400	9.37 (-4)	4.63 (-1)	9.63 (-4)	4.64 (-1)	5.42 (-15)	4.70 (-1)	6.39 (-15)	4.64 (-1)			
500	8.92 (-4)	4.10 (-1)	9.20 (-4)	4.11 (-1)	5.12 (-15)	4.17 (-1)	6.08 (-15)	4.11 (-1)			
600	7.95 (-4)	3.84 (-1)	8.21 (-4)	3.85 (-1)	4.56 (-15)	3.91 (-1)	5.42 (-15)	3.85 (-1)			
700	7.40 (-4)	3.57 (-1)	7.66 (-4)	3.57 (-1)	4.24 (-15)	3.64 (-1)	5.04 (-15)	3.58 (-1)			
800	7.00 (-4)	3.34 (-1)	7.25 (-4)	3.34 (-1)	4.00 (-15)	3.41 (-1)	4.77 (-15)	3.35 (-1)			
900	6.94 (-4)	3.11 (-1)	7.18 (-4)	3.11 (-1)	3.96 (-15)	3.17 (-1)	4.73 (-15)	3.11 (-1)			
1000	7.10 (-4)	3.12 (-1)	7.38 (-4)	3.14 (-1)	4.06 (-15)	3.19 (-1)	4.84 (-15)	3.13 (-1)			
Detector 8											
100	3.25 (-4)	5.34 (-1)	3.42 (-4)	5.39 (-1)	1.87 (-15)	5.45 (-1)	2.22 (-15)	5.37 (-1)	1.17 (+1)	0.0	4.64 (+2)
200	3.10 (-4)	3.93 (-1)	3.23 (-4)	3.96 (-1)	1.76 (-15)	4.00 (-1)	2.11 (-15)	3.95 (-1)			
300	3.06 (-4)	2.98 (-1)	3.18 (-4)	3.02 (-1)	1.74 (-15)	3.04 (-1)	2.09 (-15)	3.00 (-1)			
400	2.76 (-4)	2.77 (-1)	2.87 (-4)	2.81 (-1)	1.57 (-15)	2.84 (-1)	1.88 (-15)	2.79 (-1)			
500	3.43 (-4)	2.74 (-1)	3.55 (-4)	2.75 (-1)	1.95 (-15)	2.79 (-1)	2.33 (-15)	2.75 (-1)			
600	4.59 (-4)	3.66 (-1)	4.82 (-4	3.72 (-1)	2.64 (-15)	3.76 (-1)	3.13 (-15)	3.68 (-1)			
700	4.23 (-4)	3.44 (-1)	4.44 (-4	3.49 (-1)	2.43 (-15)	3.53 (-1)	2.88 (-15)	3.46 (-1)			
800	4.21 (-4)	3.10 (-1)	4.43 (-4)	3.14 (-1)	2.42 (-15)	3.17 (-1)	2.87 (-15)	3.11 (-1)			
900	4.06 (-4)	2.88 (-1)	4.26 (-4)	2.92 (-1)	2.33 (-15)	2.95 (-1)	2.77 (-15)	2.89 (-1)			
1000	3.97 (-4)	2.70 (-1)	4.16 (-4)	2.74 (-1)	2.28 (-15)	2.77 (-1)	2.70 (-15)	2.71 (-1)			
Detector 11											
100	1.75 (-3)	7.91 (-1)	1.85 (-3)	7.97 (-1)	1.04 (-14)	8.00 (-1)	1.20 (-14)	7.92 (-1)	1.17 (+1)	0.0	4.87 (+2)
200	8.74 (-4)	7.19 (-1)	9.20 (-4)	7.23 (-1)	5.18 (-15)	7.30 (-1)	5.98 (-15)	7.20 (-1)			
300	6.49 (-4)	6.41 (-1)	6.83 (-4)	6.46 (-1)	3.81 (-15)	6.55 (-1)	4.44 (-15)	6.43 (-1)			
400	5.53 (-4)	5.80 (-1)	5.82 (-4)	5.85 (-1)	3.24 (-15)	5.95 (-1)	3.78 (-15)	5.82 (-1)			
500	4.92 (-4)	5.30 (-1)	5.18 (-4)	5.34 (-1)	2.86 (-15)	5.44 (-1)	3.36 (-15)	5.31 (-1)			
600	4.87 (-4)	4.92 (-1)	5.11 (-4)	4.96 (-1)	2.82 (-15)	5.06 (-1)	3.32 (-15)	4.94 (-1)			
700	4.42 (-4)	4.59 (-1)	4.68 (-4)	4.63 (-1)	2.58 (-15)	4.73 (-1)	3.05 (-15)	4.16 (-1)			
800	4.19 (-4)	4.27 (-1)	4.38 (-4)	4.31 (-1)	2.42 (-15)	4.39 (-1)	2.86 (-15)	4.28 (-1)			
900	4.07 (-4)	3.97 (-1)	4.26 (-4)	4.01 (-1)	2.34 (-15)	4.09 (-1)	2.77 (-15)	3.99 (-1)			
1000	4.07 (-4)	3.64 (-1)	4.26 (-4)	3.67 (-1)	2.34 (-15)	3.75 (-1)	2.77 (-15)	3.65 (-1)			
Detector 14											
100	3.07 (-4)	3.96 (-1)	3.19 (-4)	3.98 (-1)	1.75 (-15)	3.99 (-1)	2.09 (-15)	3.97 (-1)	1.17 (+1)	0.0	5.20 (+2)
200	2.15 (-4)	3.05 (-1)	2.23 (-4)	3.06 (-1)	1.22 (-15)	3.09 (-1)	1.46 (-15)	3.06 (-1)			
300	2.37 (-4)	3.29 (-1)	2.47 (-4)	3.31 (-1)	1.35 (-15)	3.35 (-1)	1.61 (-15)	3.30 (-1)			
400	2.14 (-4)	2.82 (-1)	2.24 (-4)	2.84 (-1)	1.22 (-15)	2.87 (-1)	1.46 (-15)	2.83 (-1)			
500	2.78 (-4)	3.64 (-1)	2.86 (-4)	3.58 (-1)	1.58 (-15)	3.65 (-1)	1.89 (-15)	3.65 (-1)			
600	2.56 (-4)	3.32 (-1)	2.64 (-4)	3.27 (-1)	1.45 (-15)	3.33 (-1)	1.74 (-15)	3.33 (-1)			
700	2.80 (-4)	3.16 (-1)	2.90 (-4)	3.13 (-1)	1.60 (-15)	3.18 (-1)	1.91 (-15)	3.17 (-1)			
800	2.76 (-4)	2.85 (-1)	2.86 (-4)	2.82 (-1)	1.57 (-15)	2.87 (-1)	1.88 (-15)	2.85 (-1)			
900	2.61 (-4)	2.74 (-1)	2.71 (-4)	2.71 (-1)	1.48 (-15)	2.76 (-1)	1.78 (-15)	2.74 (-1)			
1000	2.54 (-4)	2.57 (-1)	2.63 (-4)	2.55 (-1)	1.44 (-15)	2.59 (-1)	1.73 (-15)	2.57 (-1)			

propellant tank and the larger number of source regions. A total of 1000 packets was run to calculate the gamma radiation levels at 5 detector points in the low density polyethylene.

4.2 KAP-V ANALYSIS

The KAP-V neutron results for Configuration 4B are presented in Table 4-6 for each of the 25 detector locations defined in Figure 4-1. In addition to the detector coordinates and the detector numbers, Table 4-6 presents the fast neutron flux greater than the 1.5 and 2.9 Mev thresholds, the neutron heating rate in liquid hydrogen, the heating in the high density polyethylene, and the fast neutron dose rates. Two neutron dose rates are presented. The first is the dose rate in tissue rads calculated using the carbon infinite media monovariant polynomial neutron moments data as presented in Section 3.3. The second neutron dose rate was calculated by means of the modified Albert-Welton kernel. The Albert-Welton dose rate has units of ethylene rads/hour-watt. The ethylene dose rate may be converted to a tissue dose rate by multiplying by a factor of 0.7. Table 4-7 presents gamma dose rates and heating rates for Configuration 4B. Data are presented for each of the 25 detector locations defined in Figure 4-1. The three types of response data presented are (1) gamma ray heating rates in liquid hydrogen, (2) heating rates in the high density polyethylene, (3) gamma rate dose rates in units of rads (carbon)/hour-watt.

The gamma ray dose rate data and heating rate data at 16 locations in the low density polyethylene for shield Configuration 7D are presented in Table 4-8. Gamma radiation levels are presented as heating rates in liquid hydrogen, heating rates in the low density polyethylene, and gamma ray dose rates in carbon rads.

The gamma ray data previously presented for Configuration 4B and 7D are total response data for all of the source regions included in the analytical models. Tables 4-9 and 4-10 summarize the individual contributions to the gamma ray dose rate from each of the important regions in the reactor and shield mockup regions for Configurations 4B and 7D, respectively. Table 4-9 shows that at a point at the bottom of the propellant tank for Configuration 4B, 69 percent of the dose rate comes from the core, 3 percent from the "extra core" regions, and 27 percent of the dose rate from the mockup regions. "Extra core" refers

TABLE 4-6

KAP V NEUTRON RESULTS AS A FUNCTION OF RESPONSE FUNCTIONS CONFIGURATION 4B, HIGH DENSITY POLYETHYLENE

Detector No.	Detector Coordinates (cm) X	Y	Z	(E >1.5) Neutrons cm^{-2} sec-watt	(E >2.9) Neutrons cm^{-2} sec-watt	Hydrogen Heating Btu/Sec-in^3 watt	CH_2 Heating Btu/Sec-in^3 watt	Neutron Dose Rate Carbon Moments Rads (Tissue) Hr - watt	Albert Weiton Rads (Ethylene) Hr - watt
1	0.0	0.0	417.0	8.17 (+2)	2.98 (+2)	7.76 (-13)	1.02 (-12)	3.81 (-2)	1.00 (-2)
2	20.0	0.0	419.1	7.97 (+2)	2.91 (+2)	7.56 (-13)	9.91 (-13)	3.72 (-2)	9.75 (-3)
3	0.0	0.0	441.0	1.22 (+2)	5.17 (+1)	1.02 (-13)	1.34 (-13)	5.07 (-3)	8.52 (-4)
4	11.75	0.0	441.0	1.27 (+2)	5.30 (+1)	1.07 (-13)	1.40 (-13)	5.29 (-3)	9.08 (-4)
5	20.0	0.0	441.0	1.38 (+2)	5.82 (+1)	1.16 (-13)	1.53 (13)	5.77 (-3)	1.03 (-3)
6	40.0	0.0	441.0	2.15 (+2)	8.79 (+1)	1.84 (-13)	2.42 (-13)	9.14 (-3)	2.03 (-3)
7	61.1	0.0	441.0	6.50 (+2)	2.39 (+2)	6.08 (-13)	7.97 (-13)	2.99 (-2)	7.86 (-3)
8	11.75	0.0	464.0	2.71 (+1)	1.22 (+1)	2.21 (-14)	2.91 (-14)	1.10 (-3)	9.06 (-5)
9	40.0	0.0	464.0	3.85 (+1)	1.71 (+1)	3.15 (-14)	4.15 (-14)	1.57 (-3)	1.59 (-4)
10	78.8	0.0	464.0	5.47 (+2)	2.02 (+2)	5.08 (-13)	6.66 (-13)	2.50 (-2)	6.58 (-3)
11	11.75	0.0	487.3	6.35 (+0)	2.95 (+0)	5.12 (-15)	6.73 (-15)	2.55 (-4)	1.17 (-5)
12	40.0	0.0	487.3	8.58 (+0)	3.96 (+0)	6.93 (-15)	9.12 (-15)	3.46 (-4)	1.79 (-5)
13	78.8	0.0	487.3	4.25 (+1)	1.88 (+1)	3.49 (-14)	4.59 (-14)	1.74 (-3)	2.12 (-4)
14	11.75	0.0	520.0	8.46 (-1)	4.13 (-1)	6.68 (-16)	8.79 (-16)	3.34 (-5)	8.77 (-7)
15	40.0	0.0	520.0	1.08 (+0)	5.25 (-1)	8.58 (-16)	1.13 (-15)	4.28 (-5)	1.20 (-6)
16	78.8	0.0	520.0	3.50 (+0)	1.64 (+0)	2.81 (-15)	3.69 (-15)	1.40 (-4)	5.72 (-6)
17	0.0	0.0	464.0	2.63 (+1)	1.18 (+1)	2.15 (-14)	2.83 (-14)	1.07 (-3)	8.65 (-5)
18	20.0	0.0	464.0	2.87 (+1)	1.29 (+1)	2.35 (-14)	3.09 (-14)	1.17 (-3)	9.92 (-5)
19	61.1	0.0	464.0	7.95 (+1)	3.44 (+1)	6.61 (-14)	8.69 (-14)	3.29 (-3)	5.03 (-4)
20	0.0	0.0	487.3	6.19 (+0)	2.88 (+0)	4.99 (-15)	6.56 (-15)	2.49 (-4)	1.13 (-5)
21	20.0	0.0	487.3	6.68 (+0)	3.10 (+0)	5.39 (-15)	7.08 (-15)	2.68 (-4)	1.26 (-5)
22	61.1	0.0	487.3	1.49 (+1)	6.80 (+0)	1.22 (-14)	1.60 (-14)	6.06 (-4)	4.07 (-5)
23	0.0	0.0	520.0	8.28 (-1)	4.05 (-1)	6.54 (-16)	8.61 (-16)	3.26 (-5)	8.54 (-7)
24	20.0	0.0	520.0	8.32 (-1)	4.30 (-1)	6.97 (-16)	9.17 (-16)	3.48 (-5)	9.24 (-7)
25	61.0	0.0	520.0	1.68 (+0)	8.05 (-1)	1.34 (-15)	1.76 (-15)	6.68 (-5)	2.13 (-6)

Astronuclear Laboratory

TABLE 4-7

KAP V GAMMA RESULTS AS A FUNCTION OF RESPONSE FUNCTIONS CONFIGURATION 4B, HIGH DENSITY POLYETHYLENE

Detector No.	Detector Coordinates (cm) X	Y	Z	Hydrogen Heating $Btu/Sec\ in^3\ watt$	CH_2 Heating $Btu/Sec\ in^3\ watt$	Gamma Dose Rate Rads (C) /Hr Watt
1	0.0	0.0	417.0	8.59 (-14)	4.28 (-13)	1.48 (-2)
2	20.0	0.0	419.1	8.39 (-14)	4.18 (-13)	1.45 (-2)
3	0.0	0.0	441.0	4.41 (-14)	2.21 (-13)	7.66 (-3)
4	11.75	0.0	441.0	4.46 (-14)	2.23 (-13)	7.74 (-3)
5	20.0	0.0	441.0	4.55 (-14)	2.28 (-13)	7.89 (-3)
6	40.0	0.0	441.0	5.05 (-14)	2.53 (-13)	8.75 (-3)
7	61.1	0.0	441.0	6.81 (-14)	3.39 (-13)	1.18 (-2)
8	11.75	0.0	464.0	2.42 (-14)	1.23 (-13)	4.27 (-3)
9	40.0	0.0	464.0	2.70 (-14)	1.36 (-13)	4.72 (-3)
10	78.8	0.0	464.0	5.72 (-14)	2.85 (-13)	9.88 (-3)
11	11.75	0.0	487.3	1.36 (-14)	6.90 (-14)	2.40 (-3)
12	40.0	0.0	487.3	1.48 (-14)	7.48 (-14)	2.60 (-3)
13	78.8	0.0	487.3	2.36 (-14)	1.19 (-13)	4.12 (-3)
14	11.75	0.0	520.0	6.27 (-15)	3.20 (-14)	1.10 (-3)
15	40.0	0.0	520.0	6.67 (-15)	3.48 (-14)	1.18 (-3)
16	78.8	0.0	520.0	9.14 (-15)	4.64 (-14)	1.61 (-3)
17	0.0	0.0	464.0	2.42 (-14)	1.22 (-13)	4.24 (-3)
18	20.0	0.0	464.0	2.48 (-14)	1.25 (-13)	4.30 (-3)
19	61.1	0.0	464.0	3.31 (-14)	1.66 (-13)	5.77 (-3)
20	0.0	0.0	487.3	1.35 (-14)	6.85 (-14)	2.38 (-3)
21	20.0	0.0	487.3	1.38 (-14)	6.99 (-14)	2.43 (-3)
22	61.1	0.0	487.3	1.73 (-14)	8.75 (-14)	3.04 (-3)
23	0.0	0.0	520.0	6.24 (-15)	3.18 (-14)	1.11 (-3)
24	20.0	0.0	520.0	6.34 (-15)	3.23 (-14)	1.13 (-3)
25	61.0	0.0	520.0	7.48 (-15)	3.80 (-14)	1.32 (-3)

TABLE 4-8

KAP V GAMMA RESULTS AS A FUNCTION OF RESPONSE FUNCTIONS CONFIGURATION 7D, LOW DENSITY POLYETHYLENE

Detector No	Detector Coordinates (cm) X	Y	Z	Hydrogen Heating Btu/sec in^3 watt	CH_2 Heating Btu/Sec in^3 Watt	Gamma Dose Rate Rads (C) / Hr - Watt
1	0.0	0.0	417.0	6.77 (-15)	8.11 (-15)	1.19 (-3)
2	20.0	0.0	419.1	6.58 (-15)	7.89 (-15)	1.16 (-3)
3	0.0	0.0	441.0	5.08 (-15)	6.09 (15)	8.93 (-4)
4	11.75	0.0	441.0	5.07 (-15)	6.08 (-15)	8.91 (-4)
5	20.0	0.0	441.0	5.05 (-15)	6.07 (-15)	8.89 (-4)
6	40.0	0.0	441.0	5.00 (-15)	6.01 (-15)	8.80 (-4)
7	61.1	0.0	441.0	5.18 (-15)	6.22 (-15)	9.11 (-4)
8	11.75	0.0	464.0	3.98 (-15)	4.79 (-15)	7.02 (-4)
9	40.0	0.0	464.0	3.94 (-15)	4.73 (-15)	6.93 (-4)
10	78.8	0.0	464.0	4.30 (-15)	5.16 (-15)	7.56 (-4)
11	11.75	0.0	487.3	3.15 (-15)	3.79 (-15)	5.56 (-4)
12	40.0	0.0	487.3	3.12 (-15)	3.75 (-15)	5.49 (-4)
13	78.8	0.0	487.3	3.09 (-15)	3.72 (-15)	5.45 (-4)
14	11.75	0.0	520.0	2.30 (-15)	2.77 (-15)	4.07 (-4)
15	40.0	0.0	520.0	2.28 (-15)	2.74 (-15)	4.02 (-4)
16	78.8	0.0	520.0	2.24 (-15)	2.70 (-15)	3.96 (-4)

TABLE 4-9

GAMMA DOSE RATE CONTRIBUTIONS BY SOURCE REGION AT THE BOTTOM OF THE TANK* - CONFIGURATION 4B, HIGH DENSITY POLYETHYLENE

Region No.	Name	Rads (C) / Hr - Watt
1-9	Core	9.85 (-3)
14	Filler Strip	7.29 (-5)
15	Lateral Support	7.51 (-5)
16	Be Liner	5.23 (-5)
17	Be Reflector	5.08 (-4)
18	Pressure Vessel (1)	2.17 (-5)
26	Fressure Vessel (2)	4.12 (-7)
27	Pressure Vessel Dome	4.28 (-11)
19	Cluster Plate	2.33 (-7)
20	Support Plate	2.59 (-7)
21	Plenum	1.11 (-8)
22	Al Shield	2.76 (-8)
25	Shaft Shield	5.97 (-8)
24	Dome End Be Reflector	6.21 (-7)
13	Nozzle End Be Reflector	1.80 (-4)
12	Nozzle End Lateral Support	5.14 (-6)
10	Support Blocks	1.58 (-4)
	TOTAL EXTRA CORE	4.29 (-4)
29	Cluster Plate Mockup	2.04 (-4)
30	Support Plate Mockup (1)	8.14 (-4)
31	Support Plate Mockup (2)	7.61 (-5)
32	Plena Mockup (1)	2.49 (-3)
33	Plena Mockup (2)	8.50 (-5)
34	Poison Plate	2.26 (-4)
35	Pressure Vessel Mockup	1.28 (-5)
	TOTAL MOCKUP REGIONS	3.90 (-3)
	TOTAL PAX-E5 AND MOCKUP REGIONS	1.48 (-2)

*Detector No. 1, (X = 0.0, Y = 0.0, Z = 417.0 cm)

to those regions outside of the active core but within the PAX-E5 reactor, not including the mockup regions located above the reactor. Table 4-10 indicates that at the same detector point, but for the highly shielded configuration (Configuration 7D), the importance of the core has decreased to 62 percent; the importance of the "extra core" contributions has increased from 3 to 12 percent and the mockup regions contribute approximately the same amount; i.e., 26 percent.

TABLE 4-10

GAMMA DOSE RATE CONTRIBUTIONS BY SOURCE REGION AT THE BOTTOM OF THE TANK* - CONFIGURATION 7D, LOW DENSITY POLYETHYLENE

Region No.	Name	Rads (C)/Hr - Watt
1-9	Core	7.33 (-4)
14	Filler Strips	1.08 (-5)
15	Lateral Support	1.11 (-5)
16	Be Liner	7.84 (-6)
17	Be Reflector	6.89 (-5)
18	Pressure Vessel (1)	2.67 (-6)
26	Pressure Vessel (2)	5.90 (-8)
27	Pressure Vessel Dome	6.20 (-12)
19	Cluster Plate	3.31 (-8)
20	Support Plate	3.23 (-8)
21	Plenum	1.66 (-9)
22	Al Shield	3.90 (-9)
25	Shaft Shield	8.56 (-9)
24	Dome End Be Reflector	8.84 (-8)
13	Nozzle End Be Reflector	2.17 (-5)
12	Nozzle End Lateral Support	7.21 (-7)
10	Support Blocks	1.97 (-5)
	TOTAL EXTRA CORE	1.44 (-4)
29	Cluster Plate Mockup	3.75 (-6)
30	Support Plate Mockup (1)	7.33 (-5)
31	Support Plate Mockup (2)	5.81 (-6)
32	Flight Shield Mockup (1)	2.04 (-4)
33	Flight Shield Mockup (2)	1.94 (-5)
34	Plena Mockup (1)	4.00 (-6)
35	Plena Mockup (2)	1.96 (-7)
36	Poison Plate	6.44 (-7)
37	Pressure Vessel Mockup	1.74 (-7)
	TOTAL MOCKUP REGIONS	3.12 (-4)
	TOTAL PAX-E5 AND MOCKUP REGIONS	1.19 (-3)

SECTION 5. COMPARISON OF EXPERIMENTAL AND CALCULATED NEUTRON RADIATION DISTRIBUTIONS IN THE TANK AND HIGH DENSITY HYDROGEN SIMULATION (CONFIGURATION 4B)

Comparisons of experimental and calculated neutron radiation levels in the propellant tank and high density hydrogen simulation are presented in this section. These comparisons are made in varying detail in order to illustrate the validity of the computer techniques in predicting the radiation environment. The majority of the experimental neutron data were obtained for configuration 4B. Some measurements were made with configuration 11 to provide data for subtraction of the test cell background. A detailed discussion of the effect of test cell background is included in Volume I and shall not be repeated in this section.

A number of comparisons based on data from the FASTER Monte Carlo Code and the KAP-V Point Kernel Code are made in this section. The source data used in the FASTER and KAP-V codes were provided by the DOT-NAGS linked code package. The application of the FASTER, KAP-V, and DOT-NAGS codes to the experimental mockups has been covered in earlier sections and will not be covered in detail here. In this section, comparisons of neutron radiation levels in an essentially "unshielded" reactor configuration are presented. The reactor configuration mockup and radiation sources used in the MSFC tank experiment analysis are described in detail in the classified appendix.

The experimental neutron data presented in this section includes sulfur foil passive dosimeter data, Hurst dose rate dosimeter data, and U-238 fission chamber data. These data provide a comparison of computed flux greater than 2.9 Mev, fast neutron dose rate, and flux greater than 1.5 Mev.

Comparisons of experimental and calculated fast neutron radiation levels in the high density hydrogen simulation for configuration 4B are presented in Figures 5-1 through 5-7. Three fast neutron radiation quantities are presented for comparison. Figures 5-1 and 5-2 present the fast neutron flux for neutron energies greater than approximately 2.9 Mev. The next three illustrations present comparision of fast neutron flux greater than 1.5 Mev. Figure 5-6 and Figure 5-7 present fast neutron dose rates.

5.1 FAST NEUTRON FLUX (E > 2.9 Mev)

Figure 5-1 is an axial traverse of fast neutron flux (E > 2.9 Mev) as a function of penetration distance into the high density polyethylene. The experimental data, shown as a series of points connected by a dashed line were obtained from Figure 6-7 of Volume 1. The data in Figure 5-1 show that the KAP-V code results obtained from carbon moments are about 30 percent higher than the experimental data at the bottom of the tank, and predict too high a neutron flux throughout the polyethylene. In addition, the KAP results in Figure 5-1 underpredict the attenuation of the 2.9 Mev threshold flux in the high density polyethylene. The differences between the KAP-V predictions and the experimental data result, in part, from the application of carbon infinite media moments data to calculate the neutron flux.

FASTER Monte Carlo data are indicated on Figure 5-1 as a series of triangles connected by a solid line. Error bars are not included with the FASTER data because the FASTER code does not calculate a relative error associated with the cumulative number flux. At the bottom of the tank, the FASTER data is a factor of 2 lower than the experimental data. However because the attenuation in the hydrogen simulation as predicted by the FASTER code is less than that determined experimentally, FASTER agrees with the experimental data at 47 centimeters penetration to within 40 percent. The FASTER code predicts a somewhat greater attenuation through the hydrogen simulation than does the KAP-V program using carbon moments data.

Figure 5-2 presents a comparison of experimental flux from Figure 6-8 of Volume 1 and calculated fast neutron flux for energies greater than 2.9 Mev as a function of radial position on the tank hemispherical surface.

The experimental data are not corrected for background. However, the magnitude of background correction at these locations is estimated to be of the order of 30 percent as may be seen in Figure 5-1 at a point on the bottom of the tank.

The important thing to note in this figure is that the shape of the predicted distribution and the experimental distribution are in good agreement.

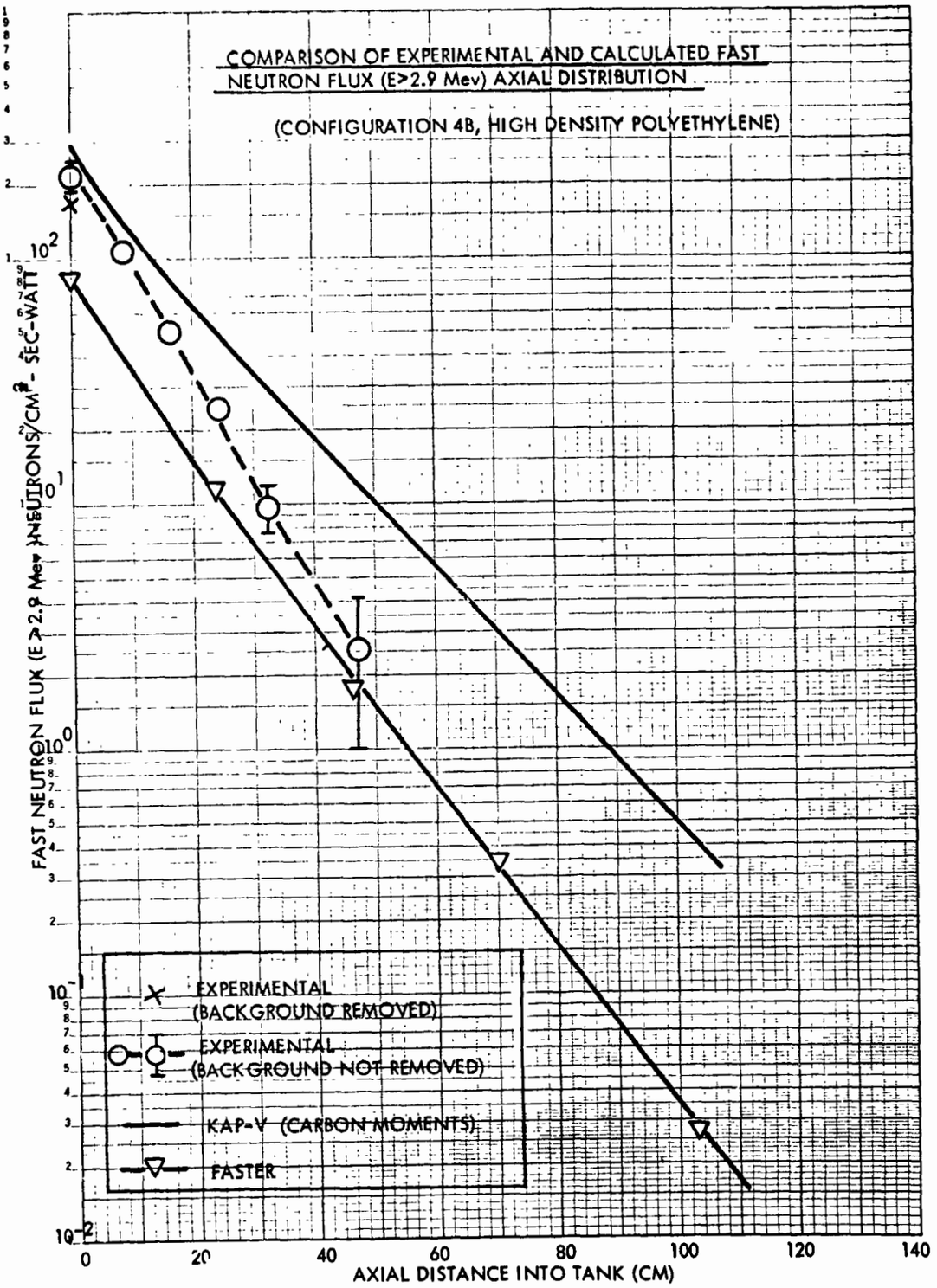

Figure 5-1. Comparison of Experimental and Calculated Fast Neutron Flux (E > 2.9 Mev) Axial Distribution

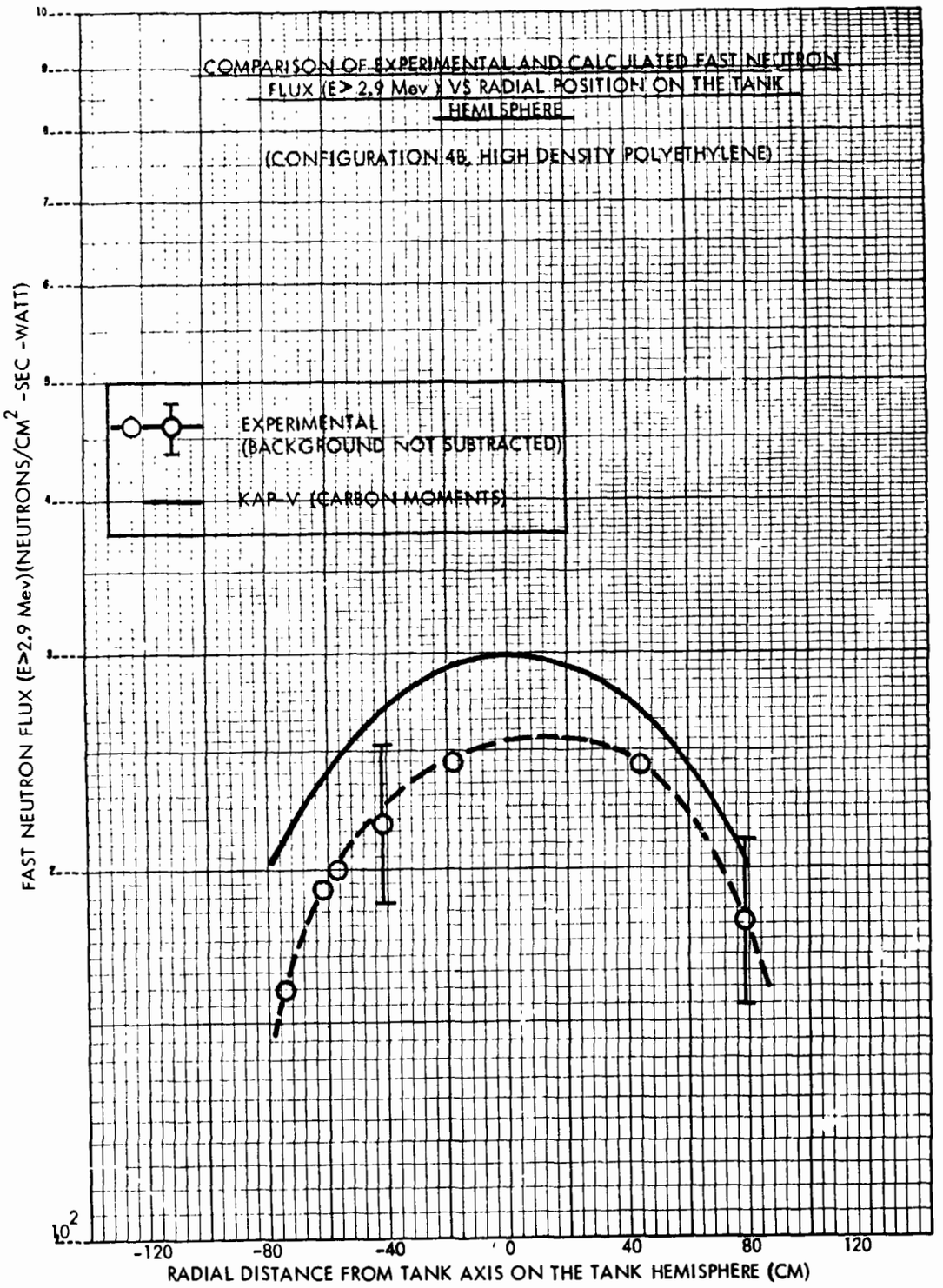

Figure 5-2. Comparison of Experimental and Calculated Fast Neutron Flux (E > 2.9 Mev) vs Radial Position on the Tank Hemisphere

5.2 FAST NEUTRON FLUX (E > 1.5 MEV)

Figure 5-3 presents a comparison of experimental and calculated fast neutron flux for energies greater than 1.5 Mev as a function of axial position in the tank. The experimental data, presented as a series of points connected by a dashed line, were obtained from Figure 6-10 of Volume 1. In this case, background was not removed. However, at two points (0 and 20 centimeters) experimental data with background subtracted are shown as X's. There is a definite anomalous behavior in the experimental data which may possibly be attributed to photo fissions in the U-238 detector. The KAP-V data, based on the carbon moments data, tend to overpredict the experimental data. At the bottom of the tank, the KAP-V result is about 50 percent higher than the corrected experimental data point. The agreement between KAP-V experimental data at 70 centimeters is fortuitous because the experimental data are questionable in this area. FASTER data are presented in Figure 5-3 without error bars because the FASTER code does not compute relative errors for the cumulative number flux.

At the bottom of the tank the FASTER result is 30 percent lower than the corrected experimental point. FASTER appears to predict a greater attenuation than is determined experimentally; however, the slope of the FASTER curve appears to be reasonable, where the experimental data is good (< 30 cm) and at large penetration depths the FASTER data are consistent.

A comparison of the experimental and calculated fast neutron flux for energies greater than 1.5 Mev is presented versus radial position in the tank in Figures 5-4 and 5-5. The experimental data in these figures was obtained from Figure 6-6 of Volume 1. The radial distributions predicted by the KAP code (Figure 5-4) are in reasonable agreement as to shape with the experimental distributions. The apparent agreement in magnitude between the KAP-V and experimental distribution at Z = 487.3 centimeters is probably fortuitous as is suggested by the axial distribution presented in Figure 5-3. The calculated and experimental distributions tend to deviate at large negative distances i.e., towards the direction of the test cell wall. The differences in shape in these areas is attributable in part to the test cell background and to the manner in which the shield mockup regions were described in the

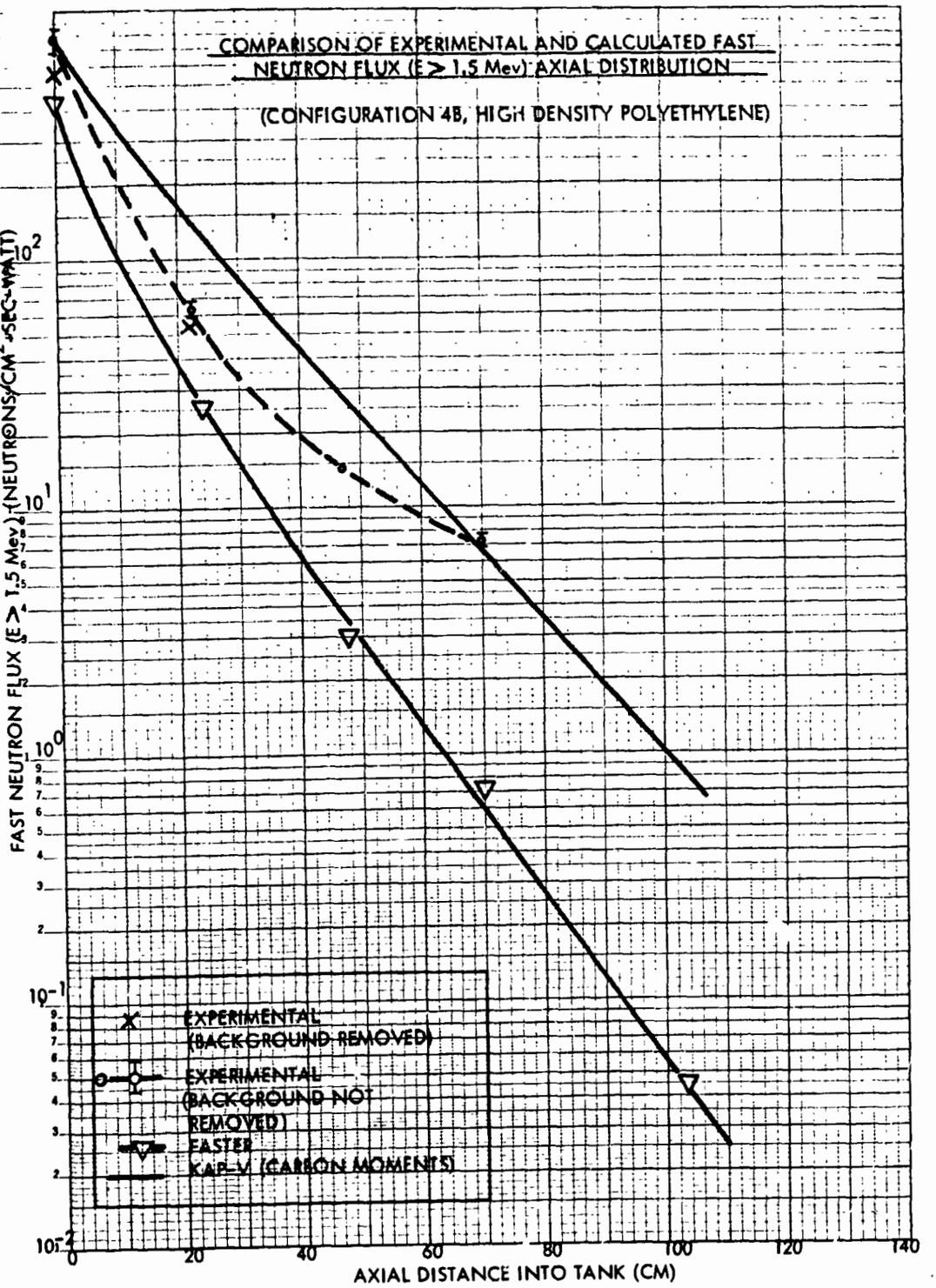

Figure 5-3. Comparison of Experimental and Calculated Fast Neutron Flux (E > 1.5 Mev) Axial Distribution

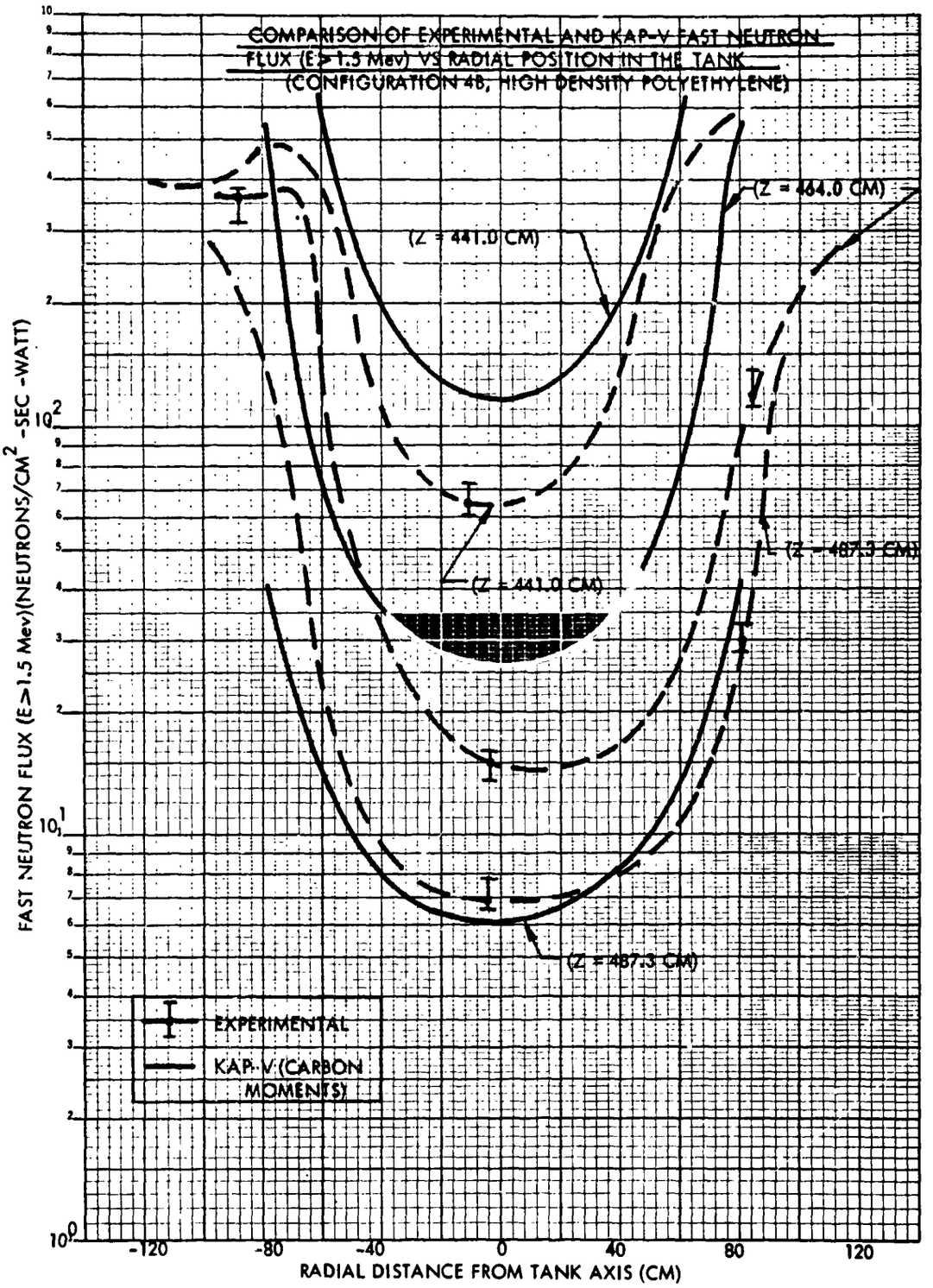

Figure 5-4. Comparison of Experimental and KAP-V Fast Neutron Flux (E > 1.5 Mev) vs Radial Position in the Tank

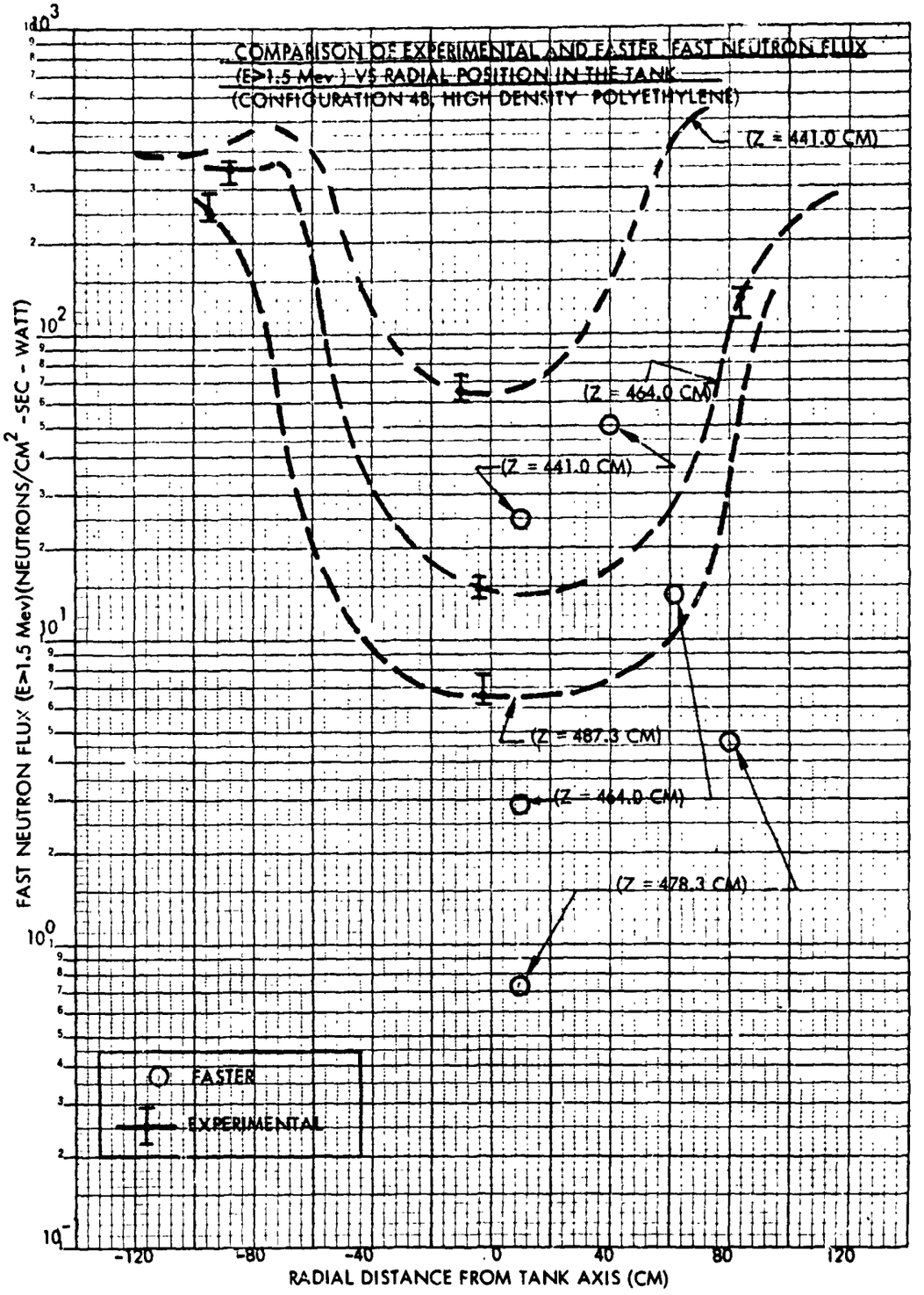

Figure 5-5. Comparison of Experimental and FASTER Fast Neutron Flux (E > 1.5 Mev) vs Radial Position in the Tank

KAP-V code. The actual shield mockup slabs had a square cross section whereas in KAP-V these regions were approximated by cylinders having areas equal to the areas of the square assemblies.

Figure 5-5 presents a similar comparison between the FASTER data and the experimental data presented in the previous illustration.

The two FASTER points located at each elevation appeared to agree with the experimentally determined spatial distributions as to shape. However, there is a significant difference between FASTER and the experiment as to absolute magnitude. However, the fault appears to lie with the experimental data as stated in the discussion of the axial traverses presented in Figure 5-3.

5.3 FAST NEUTRON DOSE RATE

Figure 5-6 presents a comparison of the experimental and calculated fast neutron dose rate on an axial distribution in the high density polyethylene. The experimental data were obtained from Figure 6-5 of Volume 1. The agreement between the experimental, FASTER,and KAP-V (Albert-Welton) dose rates is excellent. Note that the Albert-Welton dose rate was converted to units of rads tissue to permit a direct comparison with the experimental data. The fast neutron dose rate obtained from the carbon moments data appear to be too high in magnitude and underpredicts the attenuation of neutron dose in the high density polyethylene. This is to be expected since the carbon moments data do not adequately represent the neutron slowing down in a hydrogenous media.

The agreement between the FASTER results and experimental data for the fast neutron dose rate in the high density polyethylene is due to the large contribution of neutrons with energy less than 1.5 Mev. Table 5-1 presents FASTER data at the bottom of the tank where FASTER underpredicted the high energy neutron flux for energies greater than 2.9 Mev. Most of the dose rate is due to neutrons with energies less than 1 Mev. At greater penetration depths where FASTER and the experimental flux greater than 2.9 Mev agree more closely, most of the dose rate results from high energy neutrons.

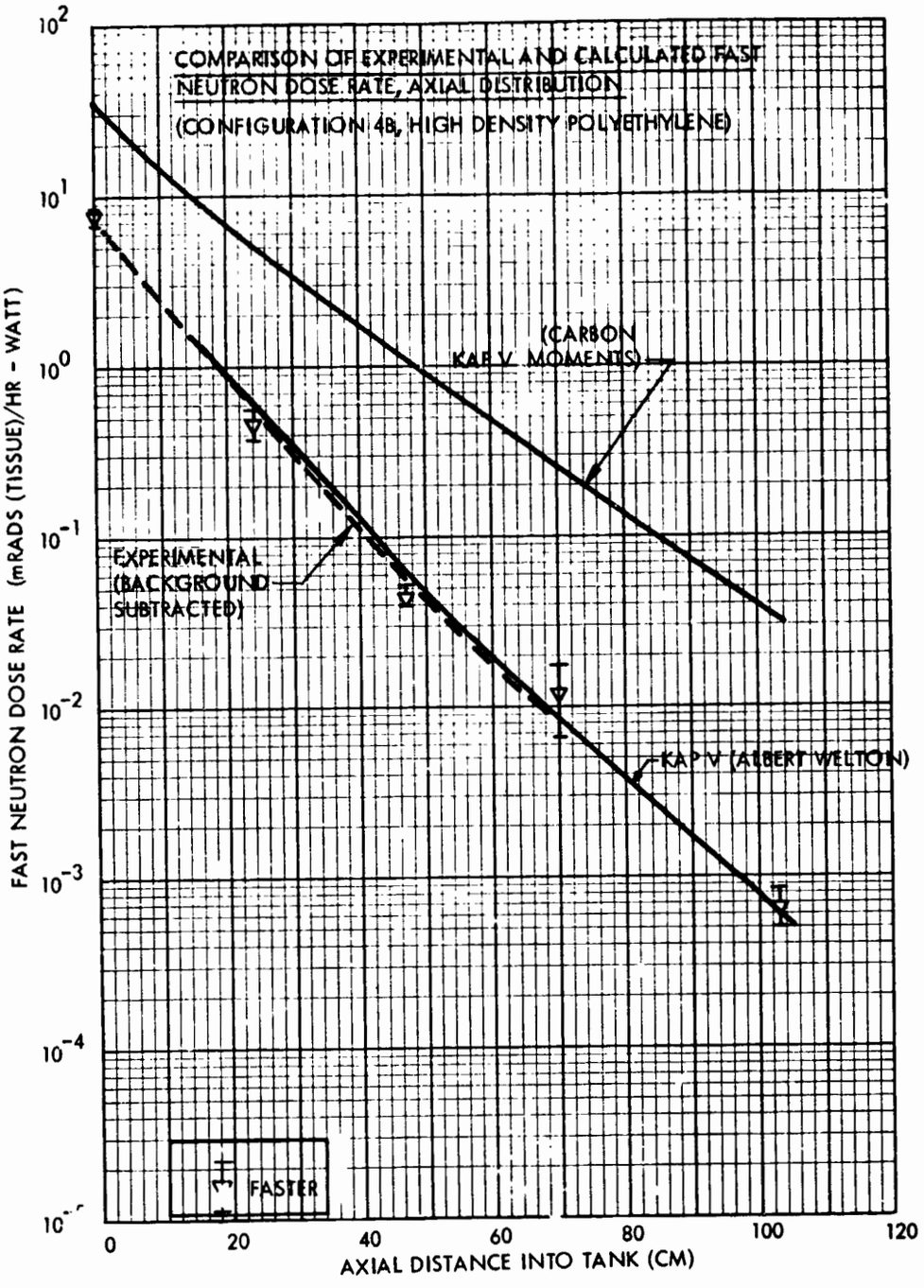

Figure 5-6. Comparison of Experimental and Calculated Fast Neutron Dose Rate, Axial Distribution

TABLE 5-1

RATIO OF NEUTRON DOSE RATE FROM NEUTRONS OF ALL ENERGIES TO THE DOSE RATE FROM NEUTRONS WITH ENERGIES GREATER THAN 1.5 Mev--CONFIGURATION 4B, HIGH DENSITY POLYETHYLENE

Detector	Dose for E > 1.5	Dose Total	Ratio: Total/ E > 1.5 Mev
1	4.73 (-3)	7.73 (-3)	1.63
4	3.24 (-4)	4.59 (-4)	1.41
8	3.19 (-5)	4.61 (-5)	1.44
11	9.50 (-6)	1.29 (-5)	1.36
14	6.02 (-6)	6.83 (-7)	1.13

The difference noted between the fast neutron dose rates obtained using the carbon moments methods and the experimental dose rates is primarily due to the presence of hydrogen in the plena mockups and tank. Carbon moments data does not adequately represent the slowing down of neutrons of 0.1 to 1.0 Mev energy in hydrogen. In computing the "effectiveness" of the other materials in terms of the dose rate attenuation effectiveness of carbon, a single "effectiveness" factor is used. Since energy dependent factors are not used, the degraded spectrum existing following penetration of a hydrogenous region cannot be constructed from the non-hydrogenous (carbon) moments data in the KAP-V code. Consequently, the use of carbon moments data will yield a spectrum characteristic of carbon, regardless of the amount of hydrogenous material penetrated. Such a calculated spectrum would, of course, have too many neutrons in the 0.1 to 1.0 Mev range and would result in an overprediction of the dose rate.

In contrast, the Albert-Welton kernel was developed specifically to describe fast neutron dose transmission in a hydrogenous medium (water). The excellent agreement between the Albert-Welton method and the measurements is readily apparent in Figures 5-6 and 5-7.

The Albert-Welton dose rate is expected to give reasonable results in the polyethylene because the Albert-Welton dose rate utilizes a hydrogen kernel. However, the excellent agreement between the Albert-Welton dose rate and experimental dose rate at the bottom of the tank is not fully understood because at this point, little hydrogen has been encountered by neutrons penetrating the mockup regions in configuration 4B.

Figure 5-7 presents the comparison of the experimental and calculated fast neutron dose rate as radial distributions at several elevations in the tank. The experimental data were obtained from Figure 6-5 of Volume 1. Near axis and off axis FASTER data points are presented together with the Albert Welton dose rate calculated by KAP-V.

As in the case of the axial traverse, the agreement between experiment, FASTER, and KAP-V (Albert Welton) data is excellent both in magnitude and shape on these radial distributions.

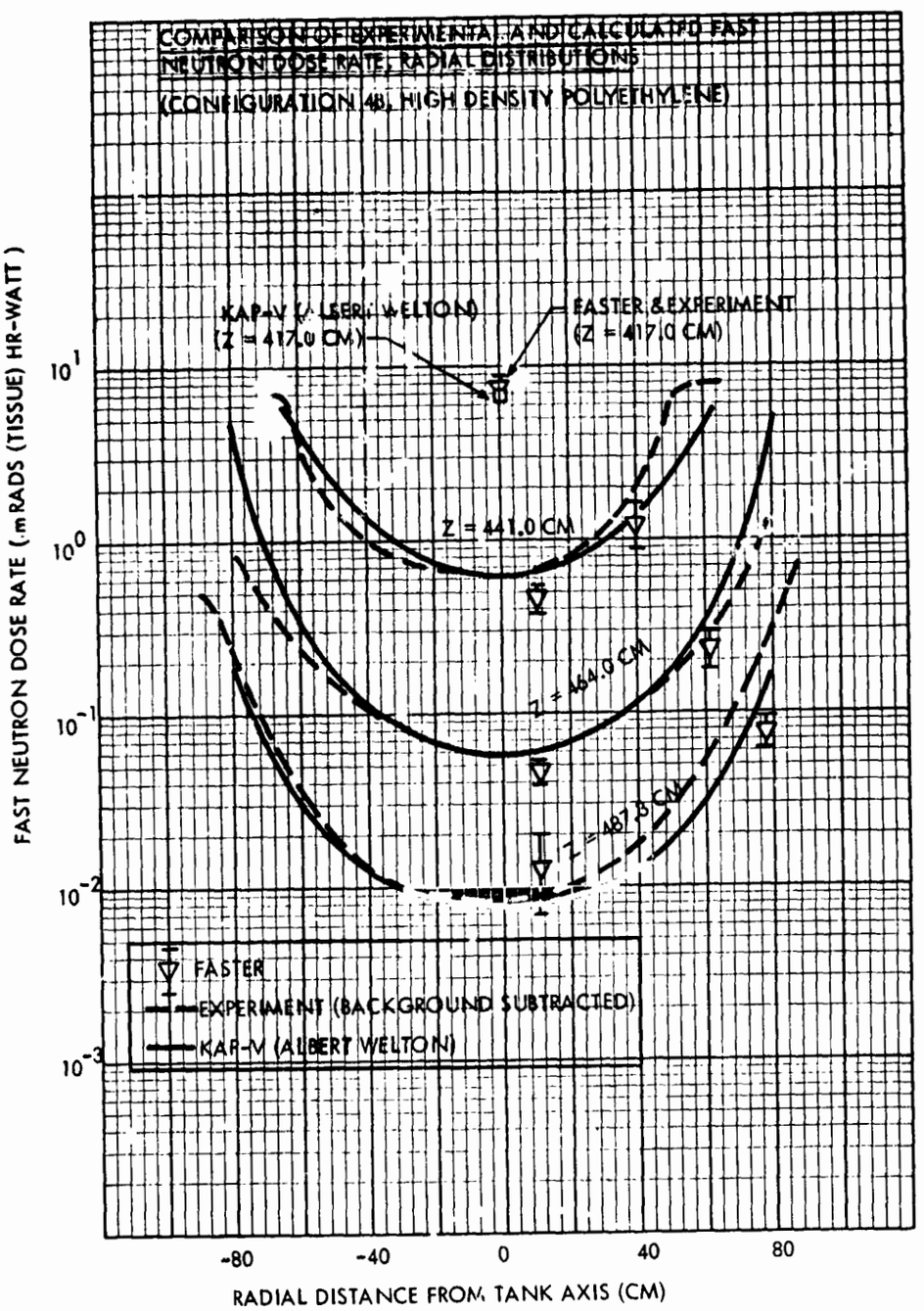

Figure 5-7. Comparison of Experimental and Calculated Fast Neutron Dose Rate, Radial Distributions

SECTION 6. COMPARISONS OF EXPERIMENTAL AND CALCULATED GAMMA RADIATION DISTRIBUTIONS IN THE TANK AND HYDROGEN SIMULATION (CONFIGURATIONS 4B and 7D)

Comparison of experimental and calculated gamma radiation levels in the propellant tank and hydrogen simulation are presented in this section. Selected experimental data obtained using calcium fluoride TLD's and a CO_2 ion chamber are presented. Calculated gamma radiation levels in the low density hydrogen simulation for shield configuration 7D and the high density hydrogen simulation for shield configuration 4B are presented since the high background encountered in the configuration 7D measurements resulted in a minimum of reliable data in the low density polyethylene. The one set of gamma dose rates presented for configuration 7D has a large experimental error associated with it. Consequently the bulk of the comparisons are made with measurements obtained in the high density polyethylene for configuration 4B.

6.1 CONFIGURATION 4B COMPARISONS

Figure 6-1 presents a comparison of experimental dose rate from Figure 6-23 of Volume 1 and calculated gamma ray dose rates in CaF_2 rads vs penetration distance into the high density polyethylene. The FASTER data and the KAP-V data appear to be in good agreement beyond a 20 centimeter penetration into the polyethylene. At the bottom of the tank the point kernel results are a factor 1.7 higher than the Monte Carlo data. The experimental and calculated attenuation through the high density polyethylene appear to be the same after a 20 centimeter penetration depth. The difference in magnitude in the experimental and calculated curves is attributable in part to the secondary gamma production in the polyethylene. The experimental data and FASTER data are in good agreement as to shape and indicates that if secondary gammas in the tank were included the analytical techniques provide good results. Figure 6-2 compares experimental and calculated gamma ray dose rates on the same traverse in units of carbon rads. These experimental data were obtained by cross plotting the data presented in Figure 6-25 of Volume 1. The point kernel calculated slope is in good agreement with the measured carbon dose rate.

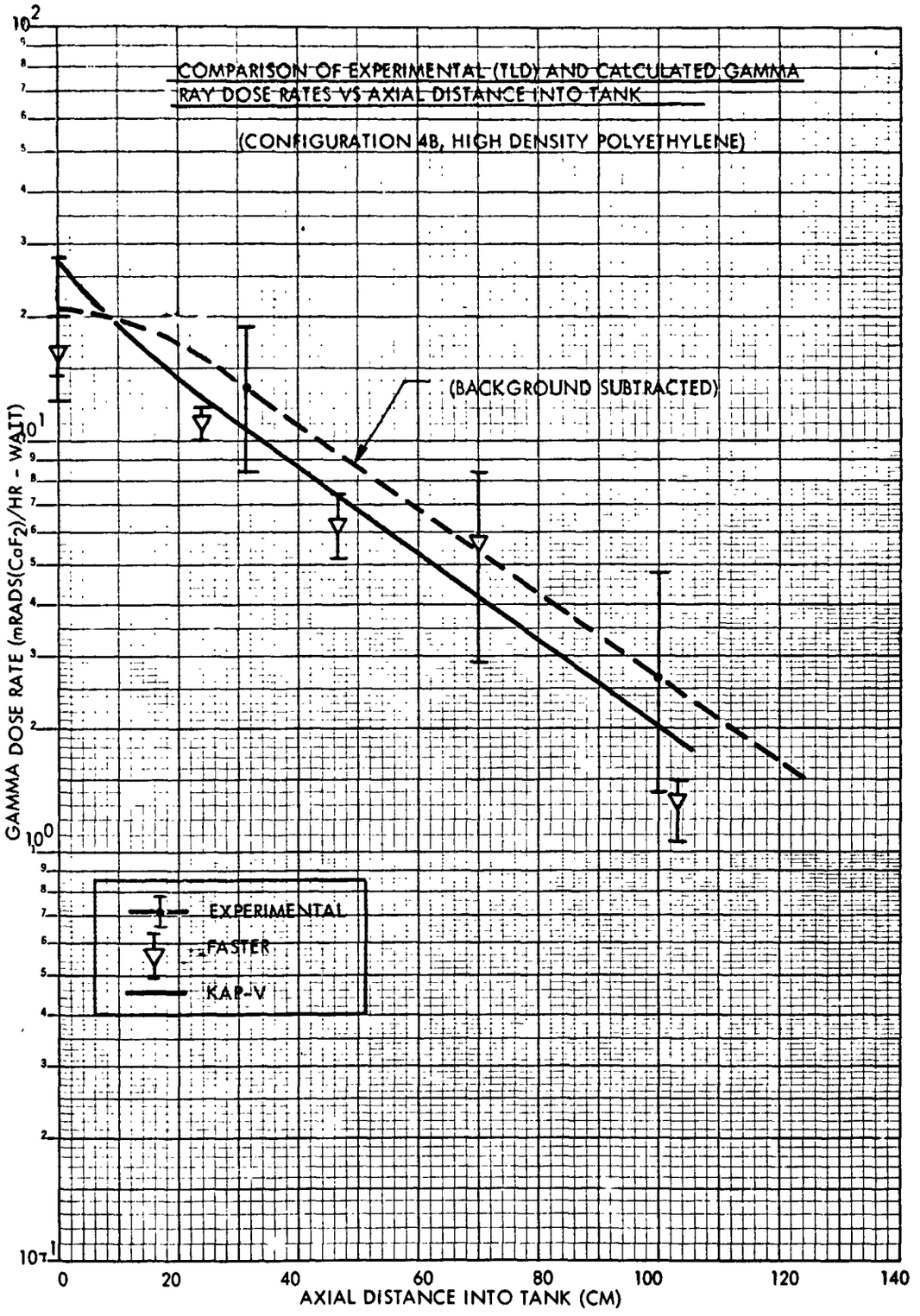

Figure 6-1. Comparison of Experimental (TLD) and Calculated Gamma Ray Dose Rates vs Axial Distance into Tank

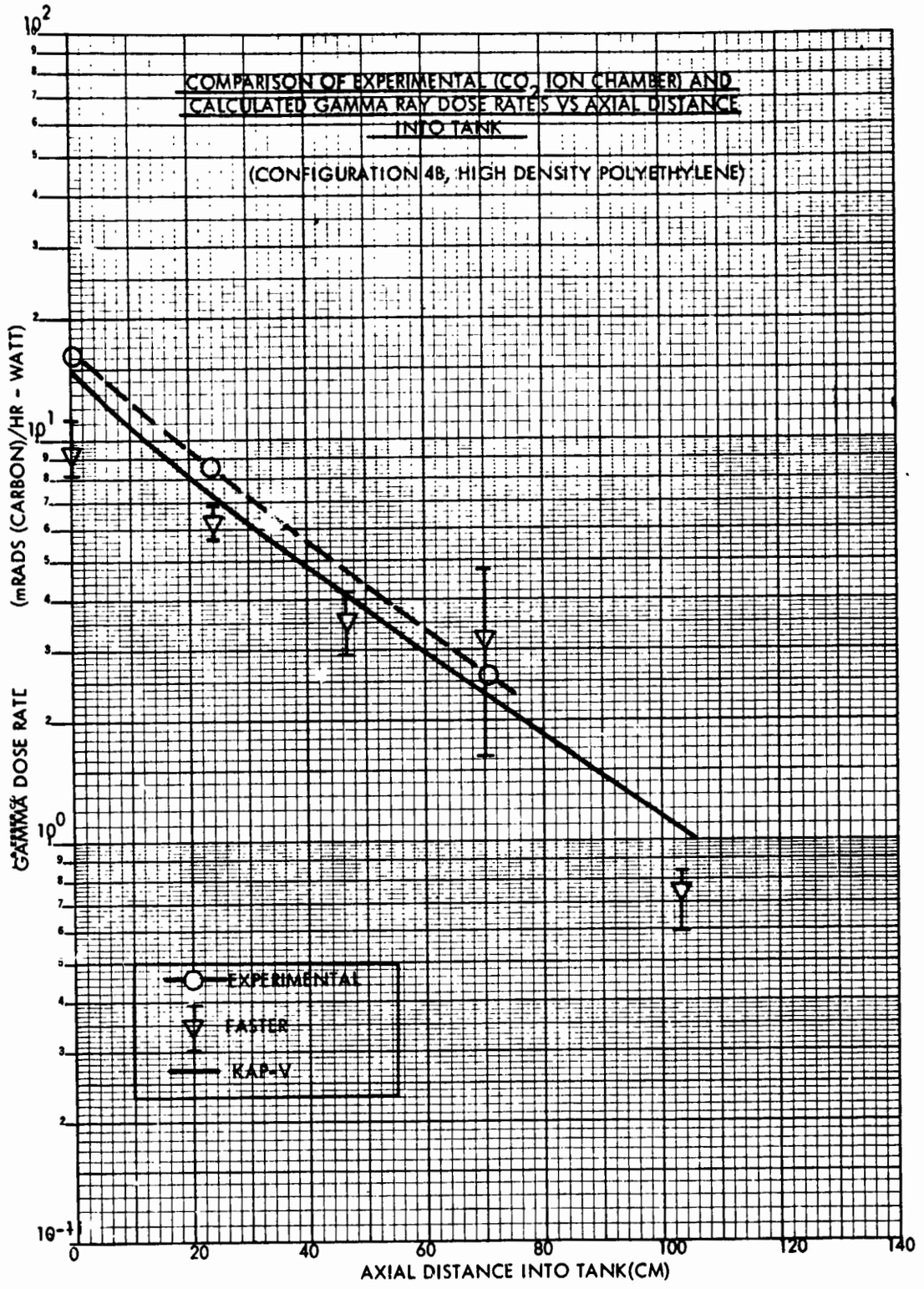

Figure 6-2. Comparison of Experimental (CO_2 Ion Chamber) and Calculated Gamma Ray Dose Rates vs Axial Distar ce Into Tank

Figure 6-3 presents comparisons of carbon rads on radial traverses at several elevations in the high density hydrogen simulation. The experimental data were obtained from Figure 6-25 of Volume 1. At the bottom of the tank, the FASTER data is a factor of 1.8 lower than the experimental data point. However, at other locations the agreement between FASTER, KAP-V, and experimental data is reasonable considering the large error bars associated with the CO_2 chamber experimental data.

Figure 6-4 compares experimental and calculated gamma dose rates on the tank hemisphere for configuration 4B. Experimental data in Figure 6-4 were obtained by using the Configuration 11 data presented in Figure 6-30 of Volume 1 to remove background from the data presented in Figure 6-20 of Volume 1. The large error bar and scatter in the experimental data prevents making a detailed comparison at these locations.

6.2 CONFIGURATION 7D COMPARISONS

Figure 6-5 compares the calculated and experimental gamma dose rates measured in the low density polyethylene for configuration 7D. Experimental data were obtained from Figure 6-34 of Volume 1. The KAP-V results are somewhat higher than the FASTER results but both calculations are in general agreement with the experimental data. The large uncertainties associated with the experimental data prevent specific quantitative comparisons.

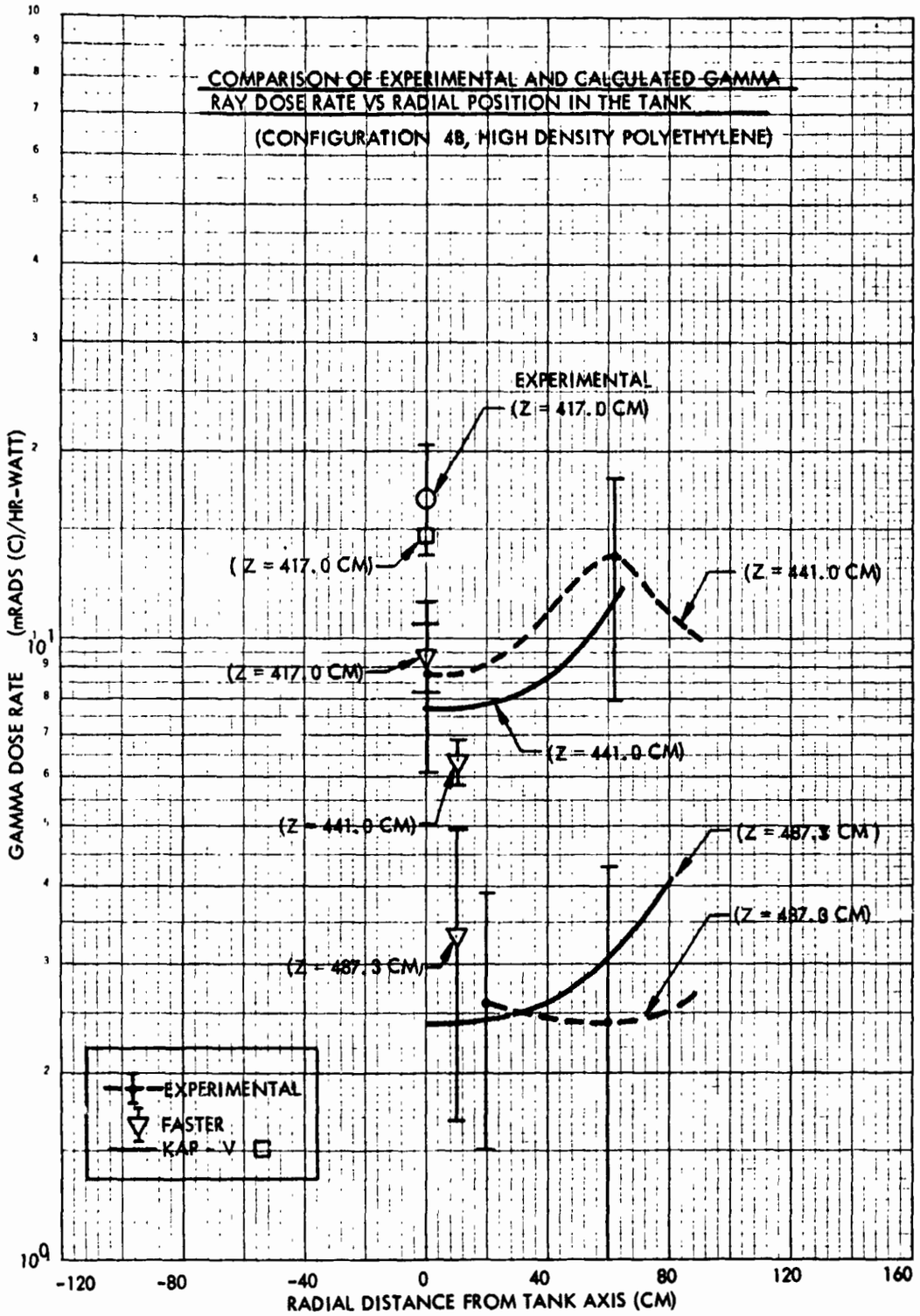

Figure 6-3. Comparison of Experimental and Calculated Gamma Ray Dose Rate vs Radial Position in the Tank

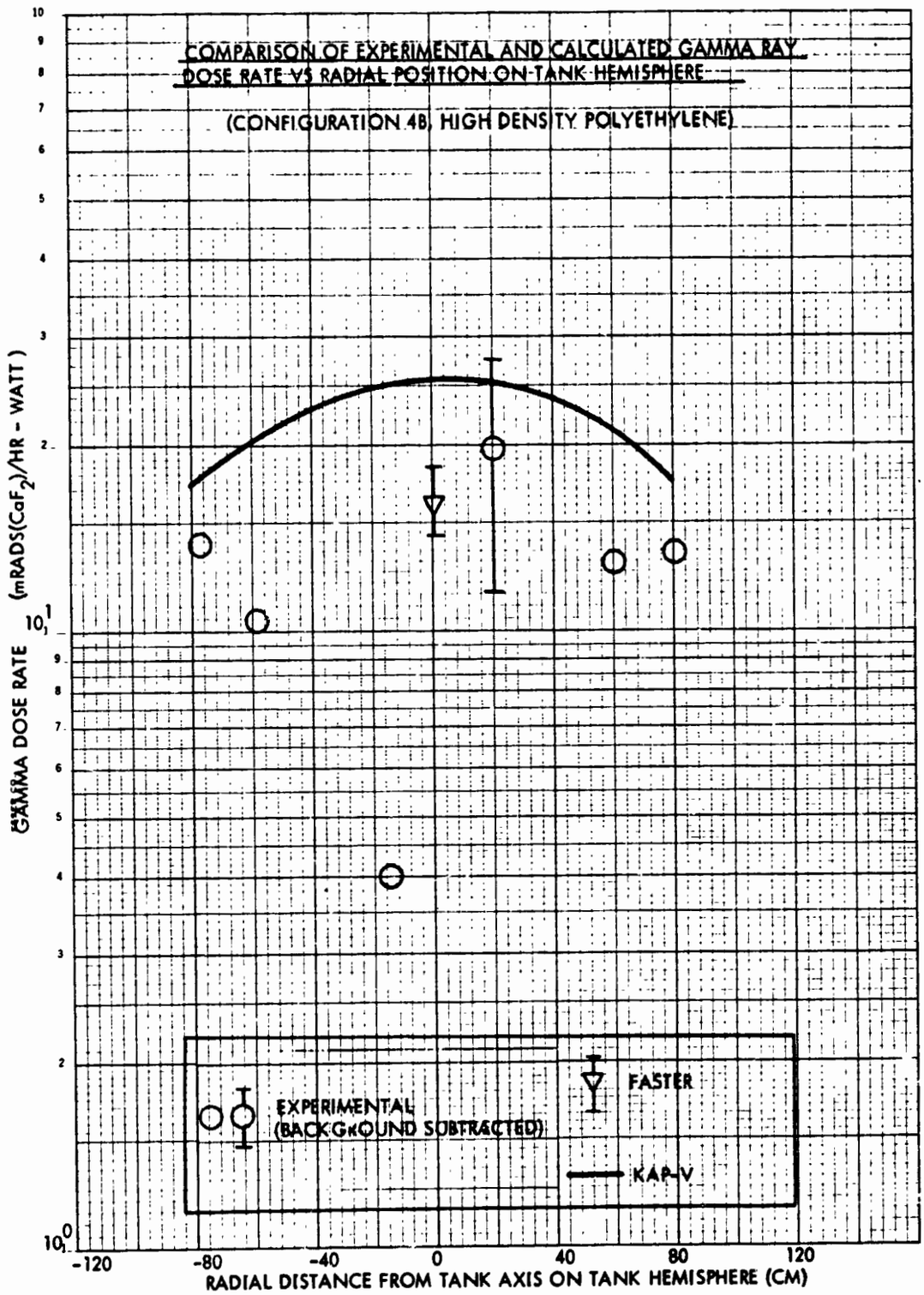

Figure 6-4. Comparison of Experimental and Calculated Gamma Ray Dose Rate vs Radial Position on Tank Hemisphere

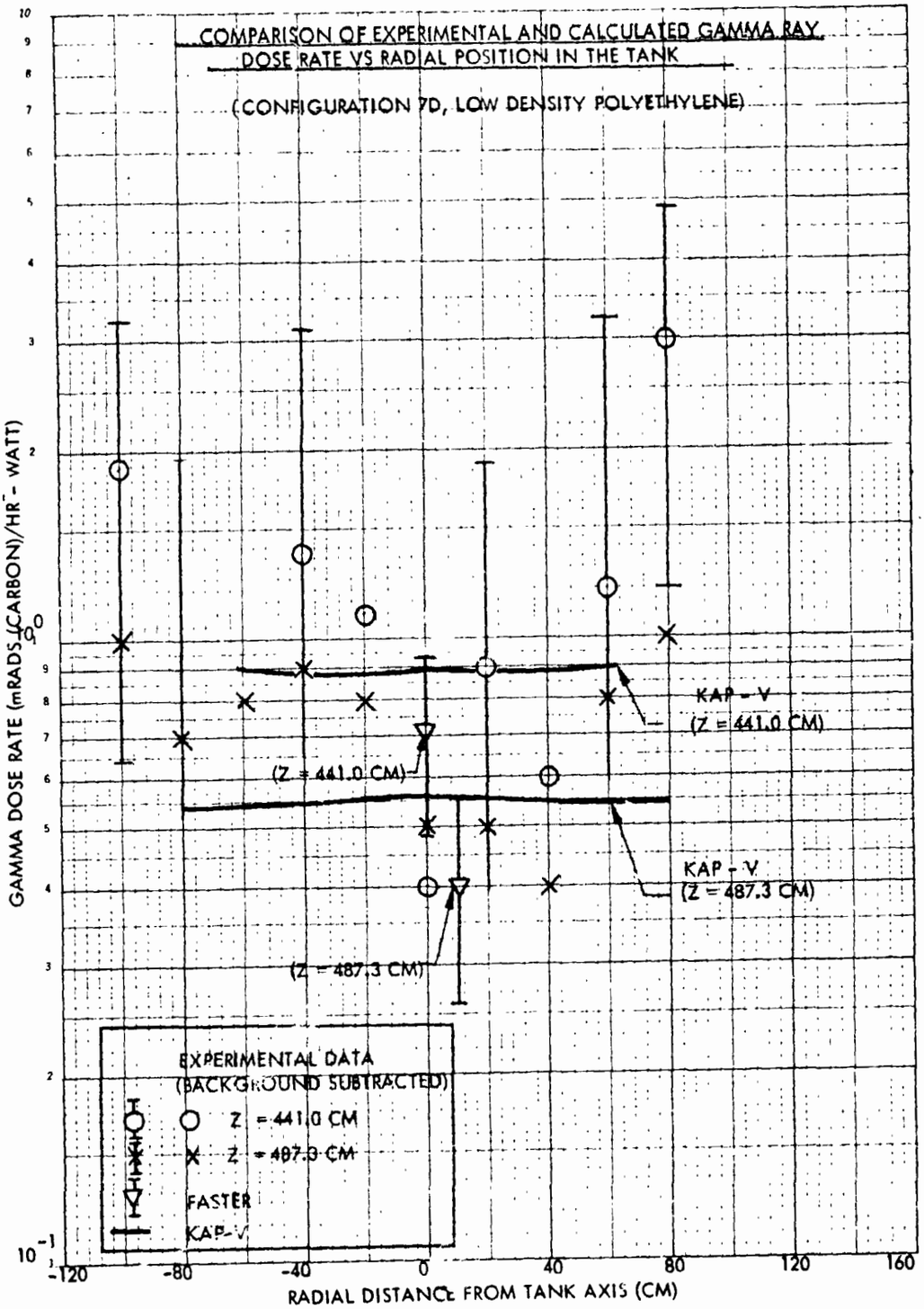

Figure 6-5. Comparison of Experimental and Calculated Gamma Ray Dose Rate vs Radial Position in the Tank

SECTION 7. INDUCED ACTIVITY AND RADIATION LEVELS AROUND GROUND TEST STAGES FOLLOWING OPERATION

The intense neutron leakage from the reactor during simulated hot firing of a nuclear rocket results in high levels of neutron induced activation of materials in the vicinity of the reactor. This activation, in turn, may result in radiation levels around the ground test stages which severely limit accessability to these areas following removal of the reactor from the test cell.

A method for calculating the induced activity in the ground test stages is demonstrated in this section. The basis for this method is the ACT II, Revised Code developed at WANL. Input requirements include material composition description and few group neutron fluxes. Output includes activation source terms in four gamma energy groups for use in subsequent dose rate calculations.

7.1 DESCRIPTION OF THE MATERIAL ACTIVATION SOURCE STRENGTH CODE, ACT-II, REVISED

The ACT-II, Revised code calculates the source strengths of radioactive materials produced by neutron irradiation. Neutron fluxes are input into the ACT code in four energy groups. The weight fractions of the material constituents (impurities), and the density of the material are required additional basic data input.

ACT-II, Revised, calculates four group gamma and five group beta source strengths in units of Mev/sec per cubic centimeter of material. A brief description of the equations solved is given below:

The activity of a nuclide being produced at a rate $\sum\emptyset$, decaying at a rate A (t) is where:

$$\lambda A(t) = \sum \emptyset \left(1 - e^{-\lambda t_o}\right) e^{-\lambda t}$$

$$\lambda A(t) = \text{source strength} \quad \frac{\text{disintegrations}}{\text{cm}^3 - \text{second}}$$

$$\sum = \text{macroscopic activation cross section cm}^{-1}$$

ϕ = neutron flux $cm^{-2}\ sec^{-1}$

t_o = irradiation time sec

λ = disintegration constant sec^{-1}

t = decay time sec

In some instances the decay product may also be unstable and produce a second generation of radioactivity. The activity of a daughter nuclide is:

where:

$$\lambda_2 B(t) = \frac{\lambda_2}{\lambda_2 - \lambda_1} A(to) \left[e^{-\lambda_1 t} - e^{-\lambda_2 t}\right] + \frac{\sum \phi}{\lambda_2 - \lambda_1} \left[(\lambda_2 (1 - e^{-\lambda_1 t_o}) - \lambda (1 - e^{-\lambda_2 t_o})\right] e^{-\lambda_2 t}$$

$\lambda_2 B(t)$ = source strength of daughter nuclide

λ_1 = disintegration constant for parent nuclide

λ_2 = disintegration constant for daughter nuclide

The source strengths, λ A or λ B, are converted to units of Mev/sec - cm^3 by the following expression:

$$S_V(E) = \lambda A(\text{or } \lambda B) \frac{\text{dis}}{cm^3 - \text{sec}} \times \gamma(E) \frac{\text{Photons}}{\text{dis}} \times (E) \frac{\text{Mev}}{\text{Photon}}$$

A more complete description of ACT-II Revised can be found in WANL-TME-598.

7.2 ACTIVATION OF PROPELLANT TANK

Input parameters for an ACT-II Revised calculation of propellant tank activation source are summarized in Table 7-1. The material composition of the aluminum alloy tank hemisphere was obtained from the spectrographic analyses of the MSFC tank materials presented in Volume I of this report. Uncertainties in the ACT calculations often are traceable to the composition description because in many materials, the trace elements or impurities may be responsible for a large part of the activation. The abundance of these impurities is often difficult to determine.

Another problem area in activation calculations lies in the determination of the neutron flux incident on and distributed within the material in question. In the present instance, a typical leakage spectrum from a sixteen group discrete ordinates calculation was normalized to the measured flux at the bottom of the MSFC tank.

The measured flux used in the normalization was the Dysprosium foil data at the bottom of the tank hemisphere obtained for configuration 4B less the background measurement obtained for configuration 11. The normalization factor developed for the thermal neutron flux agreed to within 10 percent with the fast neutron ($E > 2.9$ Mev) normalization.

Activation source strengths for the aluminum alloy of the MSFC tank are presented in Table 7-2. These data are given as a function of time after reactor operation and have as their basis a single period of reactor operation with 5.4×10^6 megawatt seconds of integrated power.

The activation source strengths in Mev/sec per cm^3 of the material are presented in two ways. First, the activity in Mev/sec attributable to each material constituent per cm^3 of material indicates the importance of the various impurities. Second, the activity in Mev/sec per cm^3 of material in each of four gamma energy groups is a convenient form for detailed dose rate and shielding calculations.

At one day after shutdown the activity results largely from the decay of short half life aluminum. At shutdown time greater than one month the activity results almost entirely from the decay of chromium, iron and zinc. It is important to note that the energy spectrum also undergoes a change with shutdown time.

7.3 DOSE RATE FROM GROUND TEST STAGES FOLLOWING SHUTDOWN

The average activation source strength in Mev/sec for an activated component may be treated as a point or distributed uniformly over a line or surface for use in calculation of dose rates. Alternately, more refined dose rate calculations may be performed by assuming a volume source distribution for use in a radiation transport computer code.

Figure 7-1 presents the dose rate after shutdown at a detector located within a few inches of the bottom of the propellant tank. Only the tank wall aluminum alloy is included in this dose rate. Also included in Figure 7-1 are activation dose rates measured in

TABLE 7-1

SUMMARY OF INPUT DATA FOR ACTIVATION CALCULATION

Operating Period: 1 hour

Power Level: 1500 MW

Shutdown Times: 0, 0.5 day, 1 day, 7 day, 30 day, 6m, 1 year

Material: Aluminum alloy (skin of MSFC tank hemisphere)

Constituents: (From Spectrographic analysis)

Element	Weight Percent
Cr	0.2*
Cu	0.09
Fe	0.19
Mn	0.45
Ni	0.005
Zn	0.03
Mg	4.80
Si	0.17
Al(balance)	94.065

*Upper Limit Used

TABLE 7-1 CONTINUED

Neutron Flux at Tank

Energy	n/cm^2 sec
E > 0.821 Mev	3.77 (12)
0.821 Mev - 5 Kev	1.01 (13)
5 Kev - 0.625 ev	1.35 (13)
E < 0.625 ev	6.00 (12)

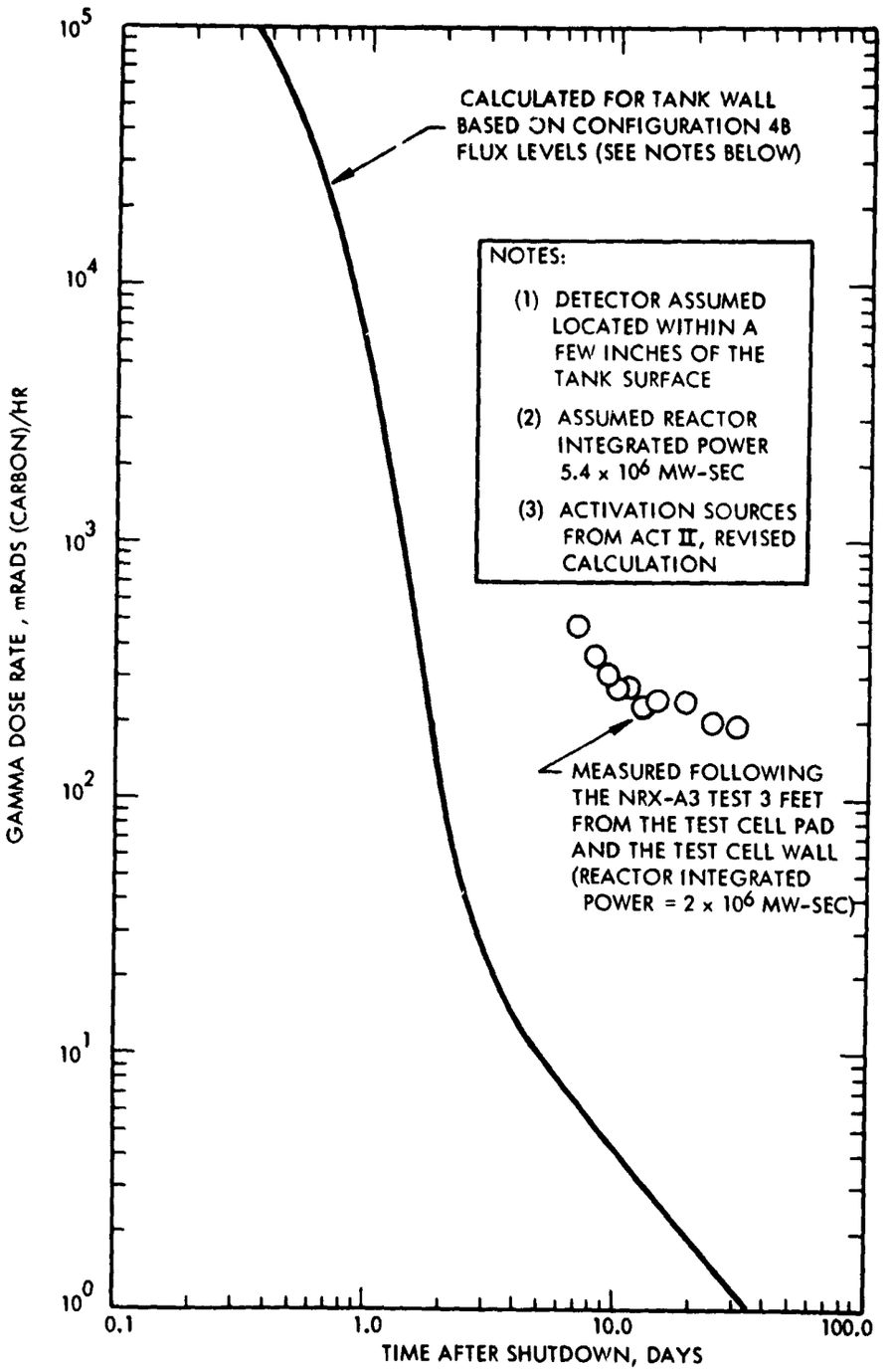

Figure 7-1. Typical Dose Rates at Bottom of Propellant Tank Resulting From Activation Sources in the Tank Wall

TABLE 7-2

ACTIVITY OF ALUMINUM ALLOY PROPELLANT TANK MATERIAL FOLLOWING ONE HOUR GROUND TEST OPERATION AT 1500 MW POWER

Activity by Constituent Gamma Activity (Mev/cm^3 - sec)

Constituent	Shutdown	12 Hr Decay	1 Day Decay	1 Week Decay	1 Mo. Decay	6 Mo. Decay	1 Yr Decay
Cr	9.572(6)	7.499(3)	7.406(3)	6.377(3)	3.532(3)	8.537(1)	-
Cu	9.795(6)	1.171(5)	6.114(4)	2.672(1)	1.604(0)	1.520(0)	1.425(0)
Fe	3.248(4)	2.219(3)	1.008(3)	8.774(2)	6.231(2)	9.423(1)	2.771(1)
Mn	5.072(9)	2.019(8)	8.034(6)	2.060(0)	1.947(0)	1.364(0)	-
Ni	1.529(4)	7.592(2)	1.958(2)	1.642(2)	1.306(2)	3.141(1)	6.170(0)
Zn	5.545(4)	3.722(4)	2.074(4)	8.206(2)	7.539(2)	4.942(2)	2.970(2)
Mg	9.062(8)	1.311(7)	7.531(6)	9.704(3)	-	-	-
Si	2.628(6)	2.345(1)	1.245(0)	-	-	-	-
Al	1.690(11)	1.371(7)	7.873(6)	1.014(4)	1.053(0)	1.053(0)	1.053(0)

Activity by Energy Group Gamma Activity (Mev/cm^3 - sec)

Energy	Shutdown	12 Hr Decay	1 Day Decay	1 Week Decay	1 Mo. Decay	6 Mo. Decay	1 Yr. Decay
0.1Mev-0.5Mev	4.932(4)	4.383(4)	2.728(4)	6.398(3)	3.537(3)	8.694(1)	1.762(0)
0.5Mev-0.9Mev	3.668(9)	1.063(8)	4.230(6)	2.184(2)	1.821(2)	6.805(1)	3.014(1)
0.9Mev-1.6Mev	5.662(8)	9.038(6)	5.185(6)	8.250(3)	1.323(3)	5.528(2)	3.022(2)
E > 1.6 Mev	1.708(11)	1.135(8)	1.409(7)	1.325(4)	2.288(0)	1.322(0)	1.074(0)
Total	1.750(11)	2.288(8)	2.353(7)	2.812(4)	5.044(3)	7.091(2)	3.352(2)

the test cell at NRDS following the NRX-A3 reactor test[14]. These measured dose rates include contributions from the test cell pad and wall concrete, steel reinforcing rods, rails, and numerous other components in the test cell area. In calculating the activation dose rate for a realistic ground test cell configuration, it is important to analyze the many components and test hardware which are present. The estimated dose rate decay curve for the tank presented in Figure 7-1 was obtained from an infinite plane source calculation and is intended to serve as an example of the use of the activation source strength data.

[14] M.A. Capo, et al., "Radiation Analysis of the NRX-A4/EST Shield Configuration" WANL-TME-1238, September 1965